Science of the Total Environment 661 (2019) 251–265

Contents lists available at ScienceDirect

Science of the Total Environment

journal homepage: www.elsevier.com/locate/scitotenv

Towards the assessment of sediment connectivity in a large Himalayan river basin

Kanchan Mishra [a], Rajiv Sinha [a,*], Vikrant Jain [b], Santosh Nepal [c], Kabir Uddin [c]

[a] Department of Earth Sciences, Indian Institute of Technology Kanpur, Kanpur 208016, India
[b] Division of Earth Sciences, Indian Institute of Technology Gandhinagar, Gandhinagar, India
[c] International Centre for Integrated Mountain Development (ICIMOD), Kathmandu, Nepal

HIGHLIGHTS

- Sediment connectivity in a large basin a function of LULC, slope and basin shape
- Integration of stream power with catchment connectivity to understand sediment dynamics
- Connectivity analysis compares well with measured sediment fluxes at the outlets.
- Spatial correspondence of IC with rainfall useful to explore functional connectivity

GRAPHICAL ABSTRACT

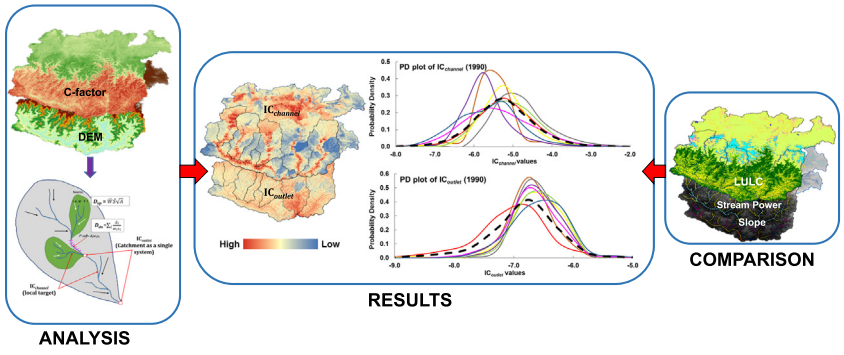

ARTICLE INFO

Article history:
Received 2 July 2018
Received in revised form 6 January 2019
Accepted 11 January 2019
Available online 14 January 2019

Keywords:
Sediment dynamics
Structural connectivity
Index of connectivity
Large rivers
Himalaya

ABSTRACT

Sediment connectivity, defined as the degree of linkage between the sediment sources to downstream areas, is one of the most important properties that control landscape evolution in river basins. The degree of linkages amongst different parts of a catchment depends mainly on the hinterland characteristics (e.g. catchment morphology, slope, shape, relief, and elevation), channel characteristics (e.g. slope, stream network density, valley confinement), and the combined effects of vegetation (e.g. land use changes and land abandonment). This paper evaluates the sediment connectivity of the upper Kosi basin covering an area of ~52,731 km^2 including Tibet and Nepal at different spatial scales. We have computed the index of connectivity (IC) using the equations originally proposed by Borselli et al. (2008) and modified by Cavalli et al. (2013) to evaluate the potential connection of sediment source areas to the primary channel network as well to the catchment outlet. Our results highlight significant spatial variability in sediment connectivity across the basin and provide important insights on structural sediment dynamics in a complex geological and geomorphological setting. We compare our results with the observed sediment load data at certain outlets and demonstrate that sediment flux in different sub-basins is controlled by variable slope distribution and land use and land cover that are strongly related to the structural connectivity. We argue that IC model can be extremely beneficial to understand sediment dynamics at catchment scale in a large river basin (~10^3–10^4 km^2 scale), where systematic field investigations for mapping hillslope-channel linkages are not feasible.

* Corresponding author.
E-mail address: rsinha@iitk.ac.in (R. Sinha).

https://doi.org/10.1016/j.scitotenv.2019.01.118

1. Introduction

In a large river system, sediment connectivity plays an essential role in understanding sediment dynamics (Fryirs, 2013), i.e., transfer of sediments between different landscape compartments designated as 'source' to 'sink.' Sediment connectivity is "the degree of coupling, the combined effect of lateral (hillslope to channel) and longitudinal (upstream river reaches to downstream) linkages between landscape components" (Heckmann and Schwanghart, 2013). Hence, sediment connectivity is an important factor that governs the mode, efficiency, and scale of sediment transfer in a catchment (Brunsden and Thornes, 1979; Harvey, 2001; Korup, 2005; Brierley et al., 2006). The spatial characterization of connectivity patterns within a catchment helps to identify sediment sources as well as to define sediment transfer paths (Cavalli et al., 2013). Therefore, the study of sediment connectivity is not only useful to develop a better understanding of sediment dynamics but it also enhances the ability to predict sediment flux in major river systems and its downstream consequences (Baartman et al., 2013).

In mountainous catchments, the concept of sediment connectivity explains the potential of sediment generation from soil erosion and remobilization of storages as well as its transfer within or between the active geomorphic zones, i.e., hillslopes and channel networks (Bracken et al., 2015). This process responds to both long-term climatic changes and short-term anthropogenic interventions (Mao et al., 2009; Macklin and Lewin, 2009). The natural factors that affect sediment transfer processes include relief, terrain roughness, stream network density, streamflow, catchment shape, erosive rainfall, sub-surface flow and soil permeability and water retention capacity (Montgomery and Dietrich, 1989; Hassan et al., 1991; Nicholas et al., 1995; Roth et al., 1996; Roy and Lamarre, 2011). In addition, several human-induced factors such as land use and land cover (LULC) changes including deforestation (Marden et al., 2005; Ward et al., 2009), afforestation (Liébault et al., 2005; Hooke, 2006; Keesstra et al., 2009), vegetation strips and agricultural drainage systems (Pavanelli and Cavazza, 2010; Pan et al., 2011; Calsamiglia et al., 2018), riparian vegetation (Keesstra et al., 2012; Poeppl et al., 2012), and land abandonment (Turnbull et al., 2008; Borselli et al., 2008; Casalí et al., 2010) as well as shallow landslides (Persichillo et al., 2017) also affect sediment transfer process within a catchment.

To develop effective sediment management strategies and to mitigate the associated hazards, several researchers have focused on the study of landscapes and sediment redistribution processes (e.g. Bracken et al., 2013, 2015) and for implementation of effective sediment trapping measures (e.g. Mekonnen et al., 2014). This has led to the development of several spatially distributed and digitally organized methods and tools to quantify connectivity at various scales (Marchi and Dalla Fontana, 2005). From plot to hillslope scale, different 'functions' (Western et al., 2001) and 'indicators' (Darboux et al., 2001; Antoine et al., 2009) have been developed to assess the connectivity. At hillslope to the catchment scale, sediment connectivity can be inferred from a conceptual framework. For example, functions like sediment delivery ratio (Walling, 1983) and sediment budgets (Bracken and Croke, 2007; Walling and Collins, 2008) have been used to provide a preliminary evaluation of catchment connectivity (Brierley et al., 2006; Baartman et al., 2013). Several indicators such as drainage density (Delmas et al., 2009), wetness index (Ali et al., 2014), and stream power index (Dalla Fontana and Marchi, 2003) have also been used to provide finer insight into the catchment connectivity. However, the spatially distributed methods such as the graph theory (Heckmann et al., 2014; Cossart and Fressard, 2017) and landscape index (Borselli et al., 2008) as well as the topographic indices (Lane et al., 2009; Cavalli et al., 2013) have proved to be useful to evaluate the sediment contribution from the different geomorphic zones of a large catchment. The latter has gained more importance because of less data requirement and has allowed the evaluation of connectivity in remote areas or in vast territories where field surveys are very difficult to carry out (Reid et al., 2007; Lane et al., 2009). It works on the topography derived from a Digital Elevation Model (DEM) and the land use maps that can be obtained from remote sensing data. This 'index of connectivity' has been widely used to assess the influence of land use changes on the sediment connectivity in Spain (López-Vicente et al., 2013; Foerster et al., 2014), to track the contaminated sediment dispersion in Japan (Chartin et al., 2013), and for the identification of hotspots of primary sediment sources to permanent sinks in an Australian semi-arid area as well as in the Mediterranean basin (Sougnez et al., 2011; Vigiak et al., 2012). Sinha et al. (2013) modeled the probable pathway of 2008 avulsion of the Kosi river in north Bihar, eastern India with the help of a topography-driven connectivity model, which largely corresponded to the observed post-avulsion scenario. The model was further used to postulate the avulsive course of the river from another upstream point based on avulsion threshold analysis (Sinha et al., 2014). Another study in the alluvial stretches of the Kosi river evaluated the spatio-temporal variation in the structural connectivity with detailed mapping of the buffers (characteristic of local slope variability, LULC map, and flow length), and the rail/road network in different years (1955, 1983, and 2010) to understand the impact of natural and anthropogenic factors on the connectivity structure (Kumar et al., 2014). Singh et al. (2017) utilized the concept of connectivity response unit (CRU) to understand the impacts of changing LULC on the connectivity structure in relatively flat terrain for both pre- and post-monsoon scenarios in water-stressed wetland Kaabar Tal in the alluvial plains of north Bihar, India. The CRU concept was further utilized by Singh and Sinha (2019) to understand the dynamic connectivity in the Kaabar wetland demonstrating that the wetland-catchment connectivity was higher for pre-monsoon compared to post-monsoon period.

Cavalli et al. (2013) modified the index of connectivity (IC) by introducing (a) D-infinity flow algorithm (Tarboton, 1997), and (b) slope modification imposing the upper limit of 1 m/m to limit the bias due to very high values of IC on steep slopes along with the residual topography; this was done by introducing roughness factor to better define the mountainous transfer properties such as debris flow and channelized sediment transfer. This led to the consideration of the different sedimentary processes that may or may not be hydrologically controlled (Bracken et al., 2015). The modified IC has been applied in the Rio Cordon catchment, Italy (Cavalli et al., 2016), Büğdüz River catchment, Turkey (D'Haen et al., 2013), and Val Müschauns valley, Switzerland (Messenzehl et al., 2014) to understand the sediment connectivity between the source and the sink. Although it has been suggested that the modified IC can be effective for large basins (Cavalli et al., 2013), where systematic field investigation for mapping hillslopes–channel linkages (Caine and Swanson, 1989; Farraj and Harvey, 2010; Theler et al., 2010) is not feasible, it is yet to be demonstrated.

In this study, the modified IC (Cavalli et al., 2013) has been applied to upper Kosi basin (UKB) including the parts of Tibet and Nepal covering an area of ~52,731 km^2. The primary objective of this paper is to develop an assessment of sediment connectivity in this large basin characterized by dominantly erosional processes that mobilize large quantities of sediments from the hinterland area to the downstream. Results of this study can have significant implications for designing sediment and flood management strategy in the transboundary Kosi River Basin.

2. Geomorphic and climatic setting of the upper Kosi basin

The Kosi River (also referred as Koshi) originates from high altitude region draining from the northern slopes of the Himalaya in the Tibet autonomous region and the southern slopes of Nepal before it finally enters the Bihar plains in India and meets the Ganga River (Fig. 1). The upper Kosi basin covers an area of ~52,731 km^2 up to Chatara (Fig. 1) with elevation varying from 164 m to 8642 m, and slope ranging from 0° to 84°. The upper Kosi basin mainly comprises Tibetan plateau,

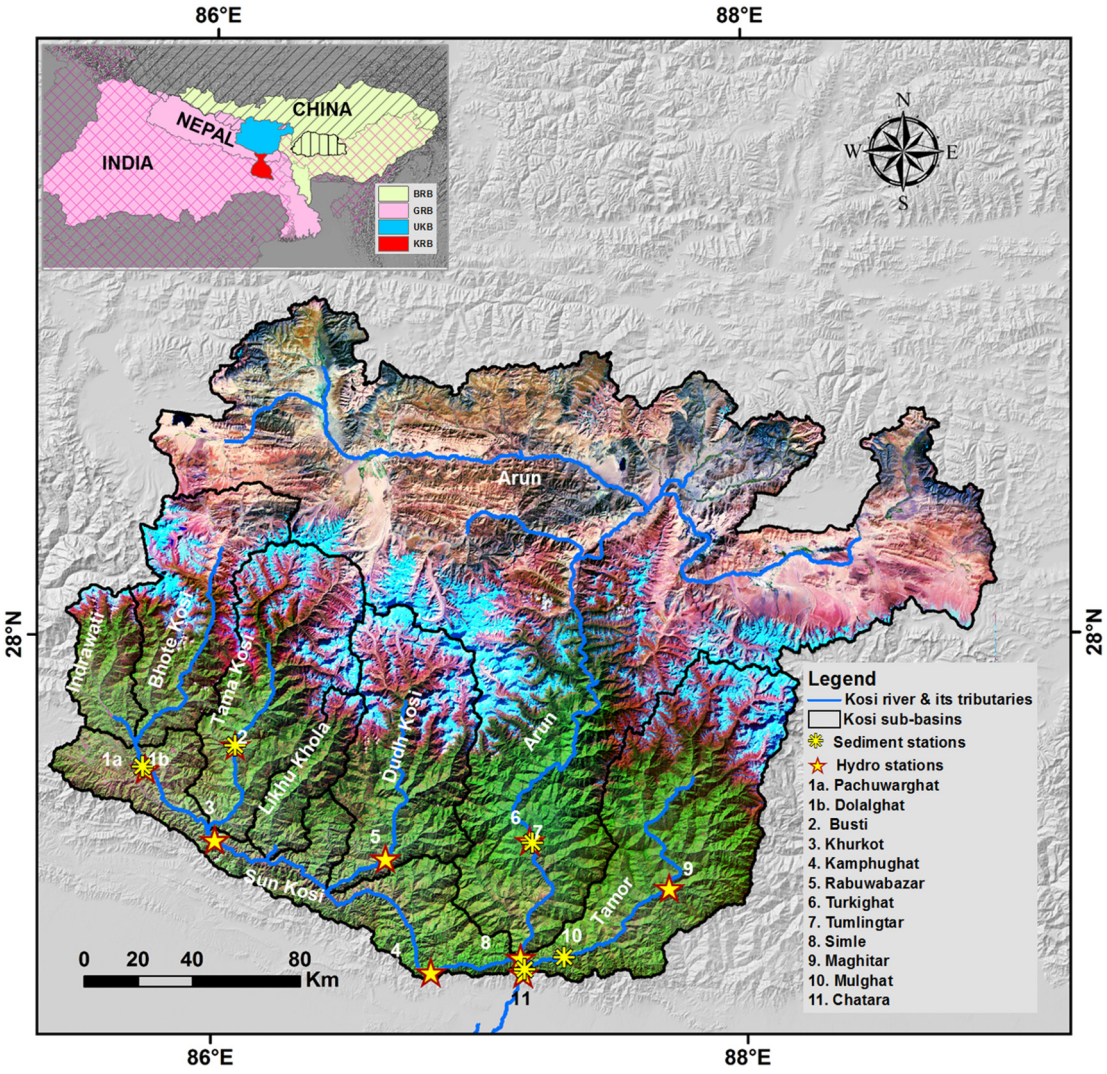

Fig. 1. The Upper Kosi river basin and the major tributaries (Note: GRB: Ganges river Basin, BRB: Brahmaputra River Basin, KRB: Kosi River Basin). The northern most part of the Kosi basin lies in Chinese part, and the remaining part in the high and middle mountains of Southern Himalaya in Nepal.

Higher and Lesser Himalaya, Siwaliks, and Terai zone. The elevated but flat Tibetan plateau in the north is characterized by numerous glaciers, glacial moraines, hummocky terrain with rounded or elongated hills and depressions. The broad U-shape glacial valleys formed due to the large-scale erosion of ice in valleys lies to its north and they acts as a source of the drainage for most of the streams of the surrounding region (Immerzeel et al., 2010). The Arun River is the main drainage system that flows through the flat valley of Tibet plateau to the mountainous region of Nepal and later joins the Sapt Kosi at Tribeni.

In the Higher Himalaya, there are permanent snow-capped mountains (~3000–8500 m), steeply dissected mountains, and hills, deep and incised rivers valleys, and tectonic basins mostly dominate these areas. It has been estimated that there are around 36 glaciers and 296 glacier lakes in the Kosi River basin (Bajracharya et al., 2007). In the Lesser Himalaya (Mahabharata range), the basin has elevations of 1000–2500 m. Major rivers such as Sun Kosi, Arun, and Tamor and their tributaries originate in the Higher Himalaya but majorly flow through the Lesser Himalayan region (Fig. 1). The Mahabharata Range acts as a barrier to the south-flowing rivers and forces the Sun Kosi and Tamor rivers to flow parallel to the range until Tribeni where they join the Arun River flowing from the north (Fig. 1). Moving to the south is the Terai zone at the northern end of the Gangetic plains with an average elevation of 100 m to 200 m above the mean sea level. The combined flow of the Sun Kosi, Arun, and Tamor (called Sapt Kosi hereafter) flows through the Barahkshetra gorge for about 15 km before emerging in the plains at Chatara (Fig. 1).

The climatic setting of the upper Kosi basin is monsoonal, and the rainfall mostly occurs in the month of June to September. Fig. 2 shows the rainfall map of the upper Kosi basin based on the APHRODITE (Asian Precipitation Highly Resolved Observational Data Integration towards Evaluation) data available at 0.25 km × 0.25 km resolution from January 1950 to December 2007 at a daily time step. The Aphrodite is a gridded precipitation data based on large number of rain gauges for Asia (Yatagai et al., 2012). With the use of MATLAB code, the gridded rainfall data was converted to the point rainfall data for the upper Kosi basin for 57 years (1950–2007). The point data sets were used to generate the rainfall map using ordinary Kriging interpolation method that assumes stationarity of the data i.e., the overall mean values and variance do not vary significantly across the study area. The rainfall map of the upper Kosi basin is marked by large regional and temporal variations in rainfall due to considerable orographic contrasts. Further, the average rainfall for each sub-basin was computed averaging the grids falling in each (Table 1). The Indrawati, Bhote Kosi, Tama Kosi, Dudh Kosi, and Sun Kosi sub-basins in the western part receive an average rainfall from 1028 to 1326 mm, whereas the Arun sub-basin in the middle part receives an average rainfall of 625 mm, which also includes the leeward side of Himalaya in the north. The Tamor sub-basin in the east receives the lowest average rainfall of 1351 mm (Table 1).

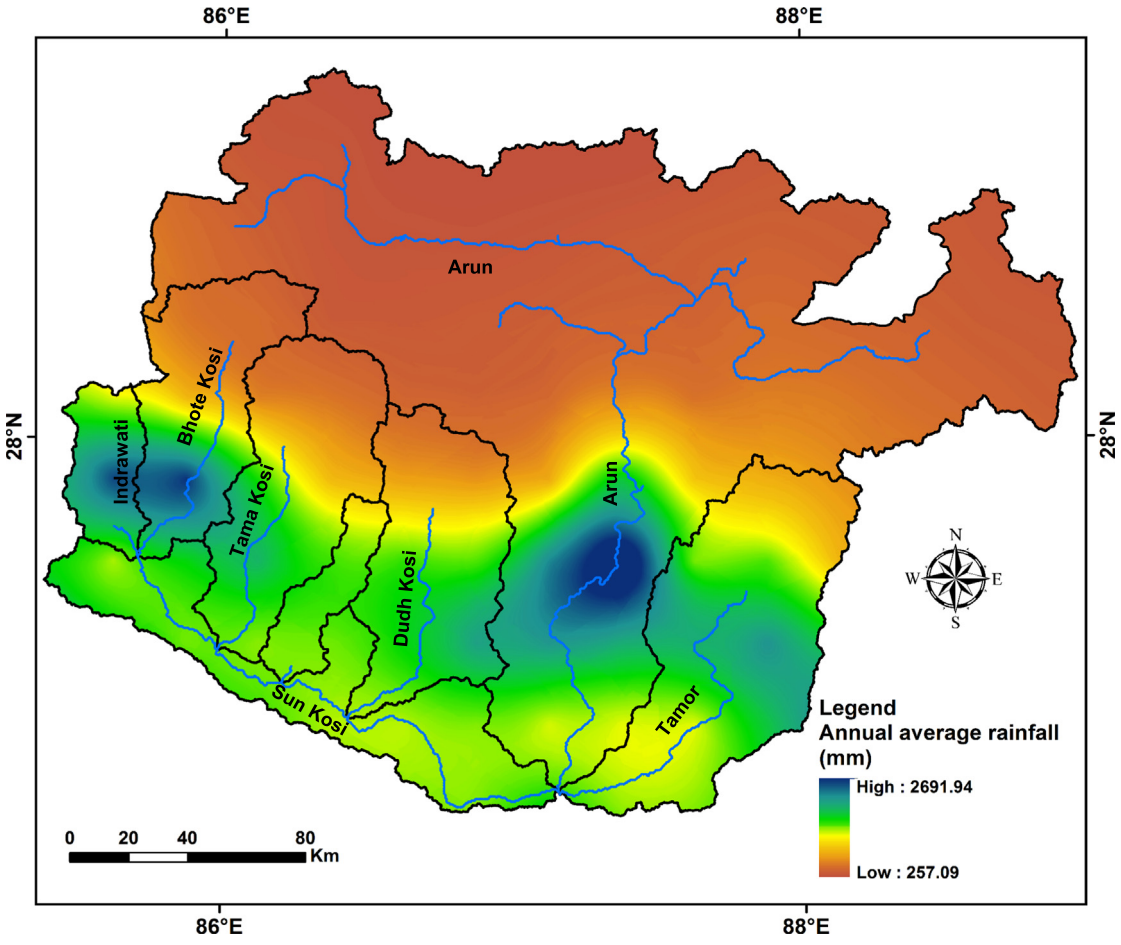

Fig. 2. Spatial variation of rainfall in upper Kosi basin based on the APHRODITE data.

3. Data and methods

3.1. Geospatial data analysis

The spatial datasets used for this study include the Digital Elevation Model (DEM), and cover management factor/crop factor, i.e., C-factor map. The hydrologically corrected DEM with a spatial resolution of 90 m derived from the Shuttle Radar Topography Mission (SRTM) data covering the upper Kosi basin corresponding to the year 2000 was used for this study.

A map of total stream power (TSP) and specific stream power (SSP) distribution in the Kosi River basin was also used to understand the results of connectivity analysis. The stream power map showing spatio-temporal distribution was derived using a physically-based hydrological model, Soil and Water Assessment Tool (SWAT) and detailed methodology has been discussed elsewhere (Kaushal et al., in prep). The method provides reach scale variation in TSP and SSP for all tributaries and trunk river of the Kosi river basin. The new method also provides temporal variability in TSP/SSP at month scale. Temporal variability is the key to understand sediment dynamics a monsoon dominated river system.

Table 1
Morphometric and hydrological characteristics of the upper Kosi basin.[a]

River	Discharge (D) and sediment station (S)	Catchment area upstream of station (km^2)	Minimum elevation[b] (m)	Average elevation[b] (m·a.s.l.)	Maximum elevation[b] (m·a.s.l.)	Average basin slope (°)	Basin average rainfall (mm/yr)	Average annual discharge (m^3/s)	Average annual sediment load (MT/year)
Bhote Kosi-Indrawati confluence	Pachuwarghat (S)/Dolalghat (D)	4842	633	3445	7774	23.52	1379	200	30
Tama Kosi	Busti (S)	3088	472	3577	7098	24.97	1028	150	10
Dudh Kosi	Rabuwabazar (D)	3717	338	3511	8642	26.08	1175	200	NA
Arun	Turkighat (D)	27,779	195	4482	8547	16.65	625	456	NA
	Simle (D)	30,380						580	
Tamor	Maghitar (D)	4391	195	2807	8216	25.91	1351	249	NA
	Mulghat (S)	5892							16
Sun Kosi	Khurkot (D)	10,000	195	1293	3596	23.64	1326	469	NA
	Kampughat (D)	17,600						864	NA
Sapt Kosi	Chatara (D; S)	52,730	164	3772	8642	20.24	898	1545	101

[a] Hydrological data compiled from Sinha et al., 2019.
[b] m·a.s.l.: meters above sea level.

Land use and land cover (LULC) map for the year 1990 was prepared from the satellite data Landsat TM and ETM+ images of 30 m spatial resolution using object-based image analysis following the methodology developed by Uddin et al. (2015). The LULC map was reclassified into 8 major classes for this work. Further, the C-Factor map corresponding to the year 1990 was generated using De Jong method (De Jong, 1994) for estimating soil erosion dynamics in the entire Kosi river basin (Uddin et al., 2016). In this method, the Normalized Difference Vegetation Index (NDVI) was calculated from the Landsat TM and ETM+ images for 1990 (nine cloud-free images taken in November to January). Then, a C-factor map for the upper Kosi basin was generated using Eq. (1) based on a simple assessment of vegetation cover, rather than a close analysis of agricultural cropping patterns (Uddin et al., 2016).

$$C = 0.431 - 0.805 * \mathrm{NDVI} \quad (1)$$

where NDVI = Near infrared (NIR) − Red (R) / Near infrared (NIR) + Red (R).

The C-factor map for the upper Kosi basin was used as the weighting factor in the sediment connectivity analysis. For the entire processing of the satelite data, the ERDAS Imagine was used and the ArcMap 10× was used for post-processing and data analysis.

3.2. Connectivity analysis

The index of flow and sediment connectivity (IC) was initially defined by Borselli et al. (2008) as follows:

$$\mathrm{IC} = \log_{10}\left(\frac{D_{up}}{D_{dn}}\right) = \log_{10}\left(\frac{\overline{W}\overline{S}\sqrt{A}}{\sum_i \frac{d_i}{w_i s_i}}\right) \quad (2)$$

where D_{up} and D_{dn} are the upslope and downslope components of connectivity, respectively, $\overline{W}$ is the average weighting factor of the upslope contributing area, $\overline{S}$ is the average slope gradient of the upslope contributing area (m/m), A is the upslope contributing area (m^2), d_i is the length of the flow path along the i^{th} cell according to the steepest downslope direction (m), w_i and s_i are the weighting factor and the slope gradient of the i^{th} cell respectively. The IC is defined in the range of $[-\infty, +\infty]$ with connectivity increasing for larger IC values ($+\infty$).

Two components of the modified (Cavalli et al., 2013), are (a) $IC_{channel}$, and (b) IC_{outlet} and they work on the same principle as proposed by the Borselli et al. (2008). However, in case of the $IC_{channel}$, the target gets defined initially (such as main river channel) for the upslope contributing area. It calculates the probability of the sediment eroded from the hillslopes to reach the nearest sink (Supplementary Fig. S1) and thus defines the hillslope to channel connectivity or lateral connectivity. For computing the IC_{outlet} (Supplementary Fig. S1), the target is set at the catchment outlet. Thus, the IC_{outlet} was calculated for each cell of the catchment by the upslope contributing area. The model calculates the optimal flow path of connectivity to the basin outlet. Further, it defines the upstream-downstream channel interaction or catchment connectivity. The IC was calculated with reference to both targets i.e., the main channel ($IC_{channel}$) and the basin outlet (IC_{outlet}) of the upper Kosi basin. For the $IC_{channel}$, the main channel of the upper Kosi basin was identified by applying a threshold value to the output of D-infinity flow accumulation followed by photo interpretation.

For the sediment connectivity analysis of the upper Kosi basin, the connectivity toolbox (http://www.sedalp.eu/download/tools.shtml) was implemented through the model builder in ArcGIS 10.X version using functionalities and algorithms available in the Spatial Analyst extension and TauDEM 4.0 tool routines (Tarboton, 1997). Now, an open source stand-alone free tool, SedInConnect (Crema and Cavalli, 2018), is also available that implements the approach developed by Cavalli et al. (2013) with the possibility of integrating surface-roughness-derived weighting factor (Cavalli and Marchi, 2008) and weighting factor normalization.

The modified IC has mostly been applied to smaller basins ranging from ~10 km^2 (Cavalli et al., 2013) to ~150 km^2 (Borselli et al., 2008) with a very high-resolution (>2.5 m) DEM. In this paper, we have applied this approach to a large basin such as the Kosi (~52,731 km^2) for the first time with a coarser DEM derived from SRTM (having ~90 m resolution) to understand the interaction between hillslopes and channels, and to the basin outlet.

Keeping in view the spatial inhomogeneties in terrain characteristics of the upper Kosi basin, we have also generated the connectivity statistics for different sub-basins (Tables 3 and 4) to understand the controlling factors of sediment dynamics better. The statistics of the $IC_{channel}$ and IC_{outlet} of the upper Kosi basin have also considered the exclusion of the IC values related to the glaciers and glacial lakes (covering ~10% of the total area), since these areas do not represent the terrain surface and they also trap sediments temporarily.

3.3. Hydrological and sediment load data analysis

The available hydrological and suspended sediment load data for the upper Kosi basin (Table 1) were compiled to evaluate and compare the results of sediment connectivity analysis. A detailed analysis of hydrology and sediment transport characteristics of the entire Kosi basin has presented elsewhere (Sinha et al., 2019, in press) and a quick summary is presented here particularly to document the sediment fluxes from different sub-basins. Table 1 highlights that the different sub-basins are of different sizes with significantly different annual discharges. Sediment data is available only for four stations and they help to assess the order of magnitude of sediment fluxes at different outlets. The final outlet of the upper Kosi basin is Chatara where an average annual sediment load of ~101 MT (Table 1) is recorded. Based on the observed data from the gauging stations, the Indrawati and Bhote Kosi (~30 MT), Tama Kosi (~10 MT), and Tamor (~16 MT) together contribute ~56% of sediment load at Chatara. The remaining ~44% of sediments is contributed by the other tributaries upstream of Chatara, namely the Arun, Dudh Kosi and Sun Kosi (Sinha et al., 2019, in press).

4. Results

4.1. Morphometry of the upper Kosi basin and stream power distribution

Fig. 3a shows the DEM and the drainage network in the upper Kosi basin with a color coding representing slope variations. The upper Kosi basin is characterized by significant variability in channel slope. The northen part (the plateau region) mostly have gently sloping reaches. In contrast, the sub-basins in the Higher Himalayan region show high channel slope up to ~22°. The lower part of the sub-basin covering the Lesser Himalaya and Siwalik region are less steeper. Fig. 3b shows the stream power distribution in the upper Kosi basin that provides an expression of the rate of energy dissipation at a given point in a river system and is inherently linked to erosion pattern and sediment transport competence (Bookhagen and Strecker, 2012). Fig. 3b is the modeled stream power distribution in the upper Kosi basin for 10 years (1985 to 1995) and it shows that the tributaries in the western part of the basin have high stream power because of the dominance of high slope variability and high rainfall. The Arun Kosi also shows low stream power in the E-W trending entire Tibetan part but high stream power in the N-S trending part draining through the Higher Himalaya and it reduces again in the lower reaches. The Tamor shows high slope variability, but the stream power is low due to lesser rainfall (and hence lower discharge, see Table 1) in this region. A detailed discussion on stream power analysis of the upper Kosi basin has been presented elsewhere (Kaushal et al., in prep).

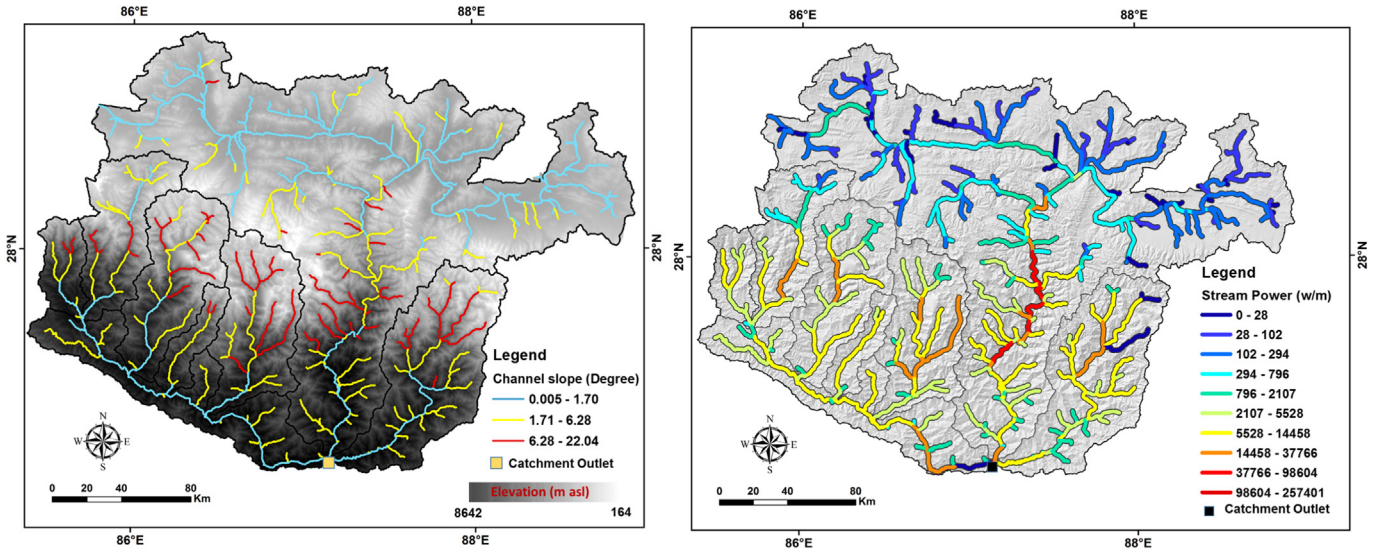

Fig. 3. (a) Spatial variation of channel slope in the upper Kosi basin; (b) modeled stream power in the upper Kosi basin using hydrological data for 10 years.

Fig. 4 shows the longitudinal profiles of all tributaries in the upper Kosi basin and highlights the varied morphology of the tributaries. The Arun has a very steep profile in most parts except for the lowermost reaches where a sharp transition to flat reaches is noted. The Bhote Kosi and Tama Kosi have very steep profiles in the uplands but they show a gradual decrease in slope in the midstream reaches. The Dudh

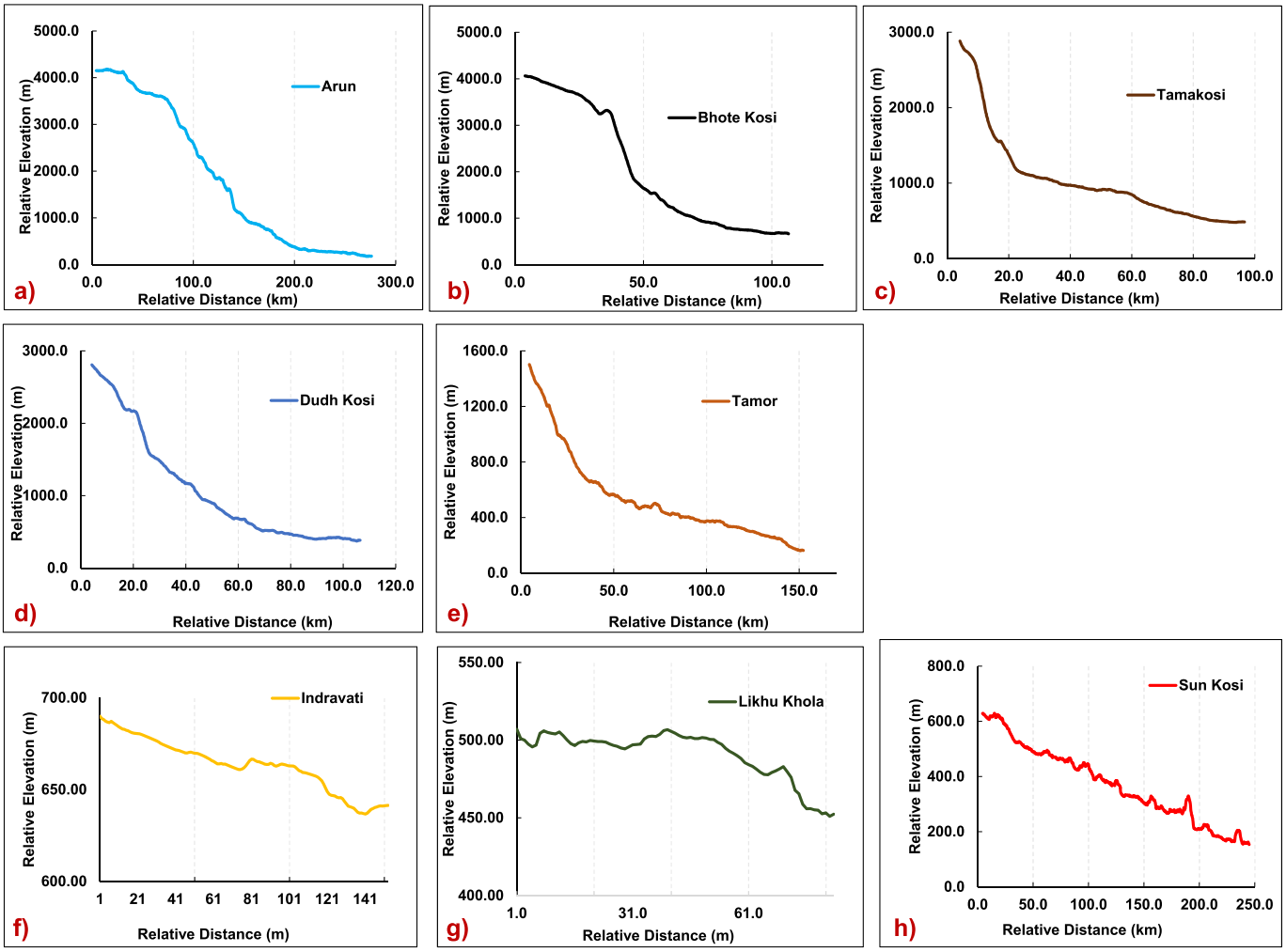

Fig. 4. Longitudinal channel profiles of major tributaries of upper Kosi basin.

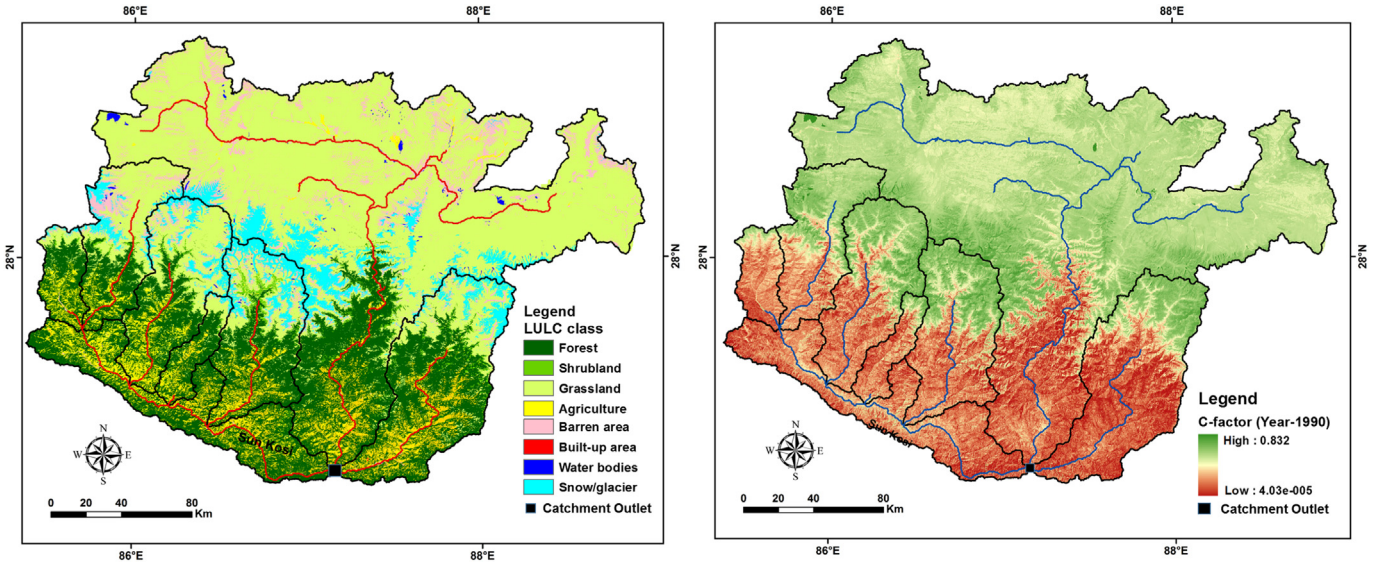

Fig. 5. (a) Land use and land cover (LULC) map of upper Kosi basin based on 1990 Landsat image; (b) C-factor map of upper Kosi basin (based on NDVI map derived from 1990 Landsat image).

Kosi and Tamor show a typical concave up profile. The Indrawati and Likhu Khola show a gradual downstream decrease in elevation but display flatter profiles close to their confluence with the Sun Kosi. The Sun Kosi shows a gradual decrease in elevation downstream with sudden breaks characterising riffle-pool sequences.

4.2. Land use and land cover (LULC) characteristics

Fig. 5a and Table 2 show the LULC map and related statistics respectively for the upper Kosi basin that clearly reflect the dominance of grasslands in the flat Tibetan plateau region. This is followed by forests (open and closed), grassland, barren areas, snow and glaciers that are widespread in the higher elevations and steep slope gradient of the Higher and Lesser Himalaya. At lower elevations in the Lesser Himalaya, a significant area under agriculture and shrubland (arable lands) are noted reflecting anthropogenic impacts in the valleys known as 'mid-lands'. Of particular interest is the variable percentage of forest and grasslands in different basins. The Arun sub-basin shows the minimum forest cover (~11%) and highest grassland area (~69%) amongst all, as a major part of the basin lies in the Tibetan part. The Sun Kosi sub-basin shows the highest forest cover (~66 %). Amongst the sub-basins of the tributaries of the Sun Kosi, the Indrawati and Likhu Khola sub-basins have relatively higher forest cover (~58%) whereas the Bhote Kosi sub-basin has a much lower (~26%) forest cover. It is also important to note that these sub-basins of the Sun Kosi namely, Bhote Kosi, Tama Kosi and Dudh Kosi have ~10% of the area covered by snow/glacier whereas the Arun and Tamor sub-basins each have 6–8% of the basin that is snow covered.

Fig. 5b shows the C-factor map of the upper Kosi basin based on the NDVI map of 1990. The continuous C-factor values obtained for the entire basin from remote sensing approach have provided estimates on a pixel-by-pixel basis which is independent of the land use class that the respective pixels belong to. The continuous C-factor map of the upper Kosi basin ranges from as low as 0.000040 to as high as ~0.832. The high mountainous areas with bare rocks (no vegetation) exhibit the highest C-factor values. Permanent snow and glaciers in the high mountainous areas were later excluded from the analysis as they have minimal contribution to the sediment connectivity in the upper Kosi basin. The areas of low C-factor values are mostly dominated by the different types of forest cover.

4.3. Hillslope to channel connectivity ($IC_{channel}$)

Fig. 6a shows the $IC_{channel}$ map of the upper Kosi basin with respect to its main tributaries. The IC values range from +4.010 (high) to −11.121 (low). Table 3 presents the statistics of the $IC_{channel}$ values for different sub-basins and highlights their spatial inhomogeneities. In the Tibetan part of the Arun sub-basin, high $IC_{channel}$ values are observed for hillslopes sloping towards north or south adjacent to the axial river running east-west of the basin (Fig. 6a) which are dominated by grassland and patches of barren areas (Fig. 5a and Table 2). Similarly, lower $IC_{channel}$ values correspond to U-shaped valleys, and piedmont fans on the eastern and western flanks of the basin that are clearly visible on satellite images. The middle part of the Arun sub-basin shows high $IC_{channel}$ values and so does the north-south trending channel, where grassland, shrubland, and barren land dominate the steep and dissected

Table 2
Land use and land cover statistics in different sub-basins of the upper Kosi basin.

Name of the basin→	Arun river	Indrawati	Bhote Kosi	Tama Kosi	Likhu Khola	Dudh Kosi	Sun Kosi	Tamor
Class name↓	Area (%)	Area (%)	Area (%)	Area (%)	Area (%)	Area (%)	Area (%)	Area (%)
Forest	11.35	57.96	26.15	32.78	58.35	39.45	65.73	48.4
Shrubland	0.52	1.2	1.44	1.73	1.19	4.45	0.5	2.6
Grassland	68.99	15.71	43.59	36.22	16.26	27.88	0.93	21.72
Agriculture	3.04	20.38	6.5	12.81	19.62	11.38	31.6	16.94
Barren area	9.39	2.33	12.08	5.88	1.23	5.88	0.72	2.64
Built-up area	0.001	0.00	0.00	0.04	0.00	0.001	0.02	0.02
Waterbodies	0.44	0.01	0.37	0.24	0.87	0.33	0.5	0.12
Snow/glacier	6.25	2.41	9.87	10.36	3.27	10.61	0.00	7.56

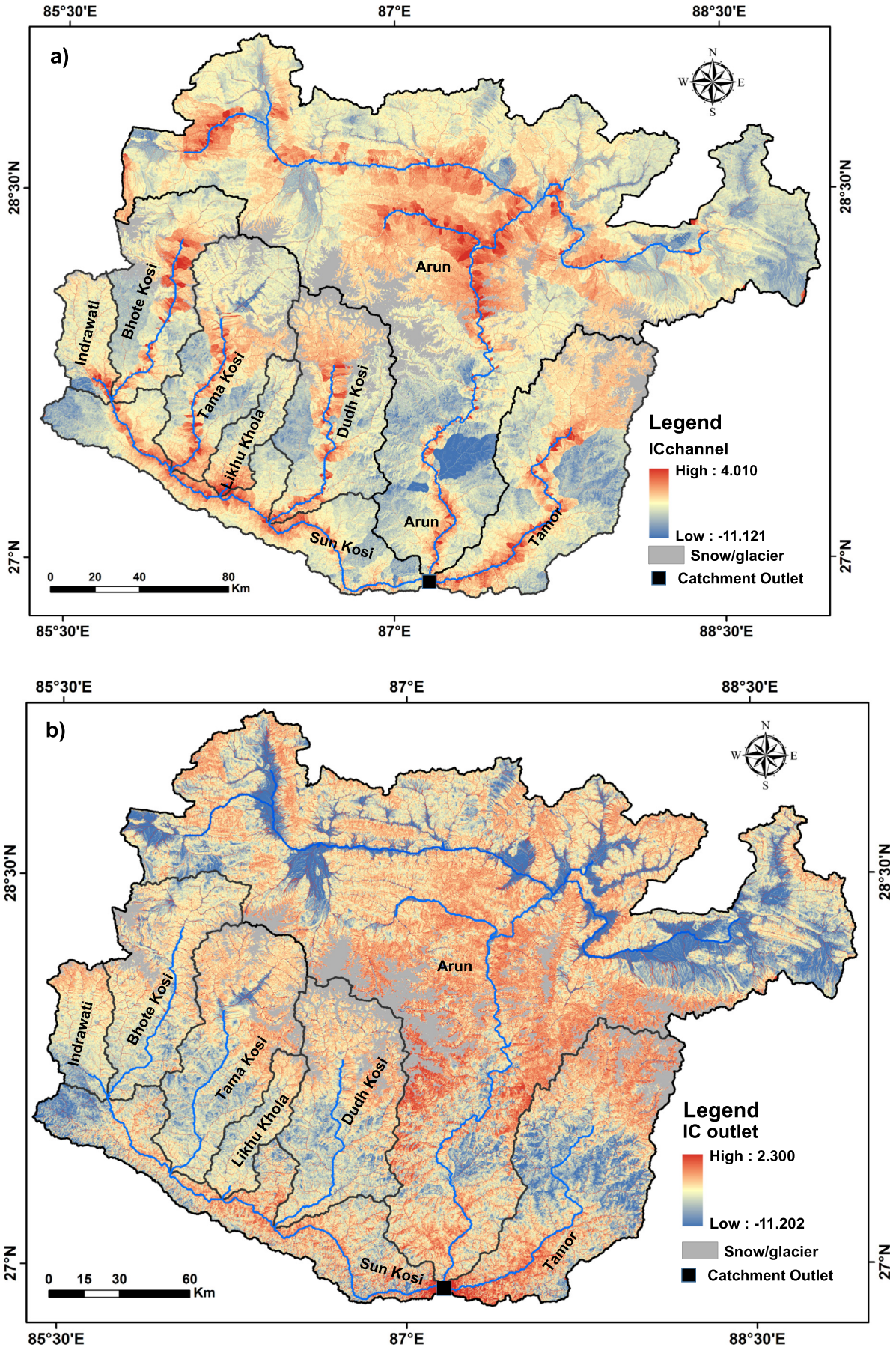

Fig. 6. (a) $IC_{channel}$ map of upper Kosi basin. (b) IC_{outlet} map of upper Kosi basin.

Table 3
$IC_{channel}$ statistics of the tributaries of the upper Kosi basin.

Name of the basin	Minimum	Maximum	Mean	Standard deviation	Median	Area % of IC under Q1[a]	Area % of IC under Q2[a]	Area % of IC under Q3[a]	Area % of IC under Q4[a]
Bhote Kosi	−8.673	3.765	−4.791	0.726	−4.904	3.71	22.10	32.85	41.33
Dudh Kosi	−9.394	3.925	−5.085	0.753	−5.162	18.71	25.28	23.09	32.92
Arun	−11.121	3.878	−5.201	0.814	−5.223	22.89	24.18	26.19	26.75
Tama Kosi	−9.767	3.951	−5.206	0.701	−5.254	17.92	30.70	29.80	21.58
Sun Kosi	−10.184	3.364	−5.363	0.949	−5.434	36.22	21.01	18.36	24.41
Indrawati	−9.457	3.610	−5.465	0.527	−5.504	18.93	59.01	15.08	6.98
Tamor	−10.150	4.010	−5.603	0.837	−5.577	43.66	21.65	22.44	12.25
Likhu Khola	−9.133	3.627	−5.681	0.585	−5.770	53.27	28.05	11.70	6.97
Upper Kosi basin	−11.121	4.010	−5.243	0.824	−5.272	25.10	25.04	24.97	24.89

[a] Q1, Q2, Q3, Q4 are quartile distribution with Q1 = 0–25%, Q2 = 25–50%, Q3 = 50–75%, Q4 = 75–100%; quartiles were determined with respect to the PD plot of the entire upper Kosi basin to maintain the uniformity across the sub-basins.

slopes. Midlands and confined narrow valleys dominate the main river channel in this stretch resulting in high $IC_{channel}$ values. However, alternate patches of moderate to low values of the $IC_{channel}$ can be seen on eastern and western slopes of the Arun sub-basin that form hilly areas having dense forest cover. The $IC_{channel}$ values increase again at ~62 km upstream of the confluence point and this is primarily attributed to significant agricultural land on the slopes in this stretch (Fig. 5a).

Amongst the tributaries of the Sun Kosi system, the westernmost Indrawati shows low $IC_{channel}$ values throughout the sub-basin. This sub-basin is characterized by dense forest (~58%) (Table 2) and snow/glacier (~2%) in the mountains and high hillslopes, which greatly impede sediment conveyance to the main channel. A few small patches of high $IC_{channel}$ values close to its confluence with the Sun Kosi are attributed to agriculture and shrubland on the low hillslopes and valleys areas that correspond to moderate to low slopes (Fig. 3a). The Bhote Kosi has a small patch of high values of the $IC_{channel}$ in the upslope area but the remaining parts of the sub-basin have much lower values except for a few patches of high values and these generally coincide with the agricultural lands on lower slopes. The Tama Kosi has moderately high $IC_{channel}$ values in the upper part of the sub-basin, a very large patch of high $IC_{channel}$ values in the middle part, and then again, a large patch of high $IC_{channel}$ values close to its confluence with the Sun Kosi. Barring the patch of snow cover/glacier (~10%) in the uppermost slopes of the Tama Kosi, most of the upslope region is characterized by grassland or barren areas with high slopes and this explains the high $IC_{channel}$ values in the upper part of the sub-basin. On the other hand, a sudden break in slope (Fig. 4c) close to the confluence point coupled with extensive agricultural lands results in high $IC_{channel}$ values in this part. The Likhu Khola is the smallest sub-basin in the western part of the Kosi basin with low values of the $IC_{channel}$; this sub-basin has moderate slopes and is mostly covered with dense forest (58%). The Dudh Kosi has a reasonably large patch of snow cover in the upper parts (~11%) but the high slopes immediately below have grasslands, shrublands and barren areas followed by forested land and then again agricultural areas on the lower slopes close to the confluence point. This has resulted in a patchy distribution of high $IC_{channel}$ values in the Dudh Kosi sub-basin. The axial part of the Sun Kosi with a very narrow valley and low slopes shows patches of high $IC_{channel}$ values around the confluence points of various tributaries along its northern slopes but the southern moderate slopes have consistently low $IC_{channel}$ values that again correspond to dense forest land cover.

The Tamor, the easternmost system of the upper Kosi basin, shows high IC values in the upslope region dominated by grassland and barren areas as well as on the slopes all along the main channel. The high hillslopes areas of Tamor sub-basin are characterized by almost ~48% of forest cover and ~8% of snow cover that contribute to moderate IC on the western slopes and low to moderate IC on the eastern slopes of the sub-basin.

We have also attempted to understand the interplay of slope and LULC on the overall IC values and our results (see Supplementary section) do not show any definite trend. In general, barren areas show the highest values of $IC_{channel}$ for all slope classes followed by water bodies, grassland/agriculture, shrubland, forest and built-up areas (see Supplementary Fig. S2).

4.4. Catchment connectivity (IC_{outlet})

Fig. 6b shows IC_{outlet} map of the upper Kosi basin with respect to the outlet and this is strikingly different from the $IC_{channel}$ map discussed above. The Tibetan part of the Arun sub-basin has characteristically low to moderate values along the main channel. In the middle part where the Arun flows in a north-south direction, only moderate values are observed which decrease further downstream. This is in sharp contrast to high $IC_{channel}$ values close to the N-S trending channel (Fig. 6a). The far away hill and valleys that lie in the eastern and western flanks of the sub-basin also show low IC_{outlet} values. These regions have very poorly developed channel section with low slopes and low annual rainfall. The lower part of the Arun sub-basin shows a sudden break in channel gradient (Figs. 3a and 4a) from steep to gentle towards downstream and therefore results in low IC_{outlet} values. The IC_{outlet} distribution is clearly reflected in the lowest mean as well as median values for the Arun sub-basin (Table 4) even though it is the largest of all sub-basins.

Table 4
IC_{outlet} statistics of the tributaries of the upper Kosi basin.

Basin	Minimum	Maximum	Mean	Standard deviation	Median	Area % of IC under Q1[a]	Area % of IC under Q2[a]	Area % of IC under Q3[a]	Area % of IC under Q4[a]
Tamor	−10.526	2.184	−6.562	0.495	−6.541	11.62	17.09	26.21	45.09
Dudh Kosi	−10.350	−3.785	−6.549	0.412	−6.554	5.86	18.38	32.93	42.83
Bhote Kosi	−10.333	1.956	−6.580	0.374	−6.590	4.21	18.53	42.28	34.98
Tama Kosi	−10.750	−4.137	−6.617	0.471	−6.596	9.00	20.94	31.28	38.78
Likhu Khola	−10.174	−4.497	−6.609	0.402	−6.618	7.42	21.31	36.15	35.12
Sun Kosi	−10.699	2.045	−6.673	0.486	−6.665	13.01	22.15	34.65	30.18
Indrawati	−10.565	2.300	−6.717	0.429	−6.730	11.50	29.26	36.01	23.22
Arun	−11.202	2.282	−7.008	0.621	−6.974	37.50	29.07	18.63	14.80
Upper Kosi basin	−11.202	2.300	−6.828	0.590	−6.799	25.01	25.02	24.95	25.02

[a] Q1, Q2, Q3, Q4 are quartile distribution with Q1 = 0–25%, Q2 = 25–50%, Q3 = 50–75%, Q4 = 75–100%; quartiles were determined with respect to the PD plot of the entire upper Kosi basin to maintain the uniformity across the sub-basins.

For the tributaries of the Sun Kosi, a common pattern is that the upper parts of all sub-basins show moderate to high IC_{outlet} values and the lower parts are characterized by low values (Fig. 6b). The channel slope map (Fig. 3a) and longitudinal profiles for these tributaries (Fig. 4) show sudden breaks in slope that nearly coincide with the transition of the IC_{outlet} values from high to low. The steeper river reaches are generally associated with narrow valleys, allowing a direct coupling between tributary valleys and the main river channel, but the elongate shape of these basins disconnects the upslope area to the downslope area by increasing the distance and time to reach the basin outlet. The Indrawati and Likhu Khola are amongst the smaller sub-basins having an elongate shape. The longitudinal profiles of these sub-basins show a gradual increase in slope with decreasing elevation (Fig. 4f and g); these sub-basins form local sinks just before the final outlet and therefore show low IC_{outlet} values. The Tama Kosi and Dudh Kosi are quite distinctive with large areas of high IC_{outlet} values in the uplands with a sharp change to lower values in the lower reaches (Fig. 6b). The deep and incised channels valleys in the uplands seem to be well connected to the outlet and this has significant implications for sediment dynamics (discussed later). The circular shape of the upland part of the Tama Kosi sub-basin allows a high and similar degree of connection from all directions of the upslope contributing area to the catchment outlet along with the high channel gradient. The Sun Kosi shows high IC_{outlet} values mostly confined to the middle part of the sub-basin and the values are low close to the confluence with the Arun and the Tamor. The longitudinal profile of the Sun Kosi shows a gradual decrease in slope from upstream to downstream with riffle-pool sequences (Fig. 4h) that create patches of low connectivity. The Tamor also shows moderate to high IC_{outlet} values in the upper parts of the sub-basin. These areas coincide with the high channel slopes (Fig. 3a) and manifest in a typical concave up profile with a major break at ~75 km from the source (Fig. 4e). On ground, this translates into a transition from steep and narrow valleys in the upper reaches to wider valleys in the lower reaches hampering the connection with tributaries. The middle and lower parts of the Tamor sub-basin therefore show low to moderate values of the IC_{outlet}.

Our analysis to understand the interplay of slope and LULC on IC_{outlet} values suggests that grassland and shrubland do not get affected much by slope variability whereas agriculture shows a decreasing trend with increase in slope. Most of the other LULC classses generally show higher conectivity with higher slopes but there is no definite trend (see Supplementary Fig. S3).

4.5. Degree of connectivity

To understand the degree of connectivity of all the sub-basins associated with the upper Kosi basin, the probability density (PD) of IC values are plotted against the IC range of the different sub-basins (Fig. 7a, b). The PD plots have allowed to distinguish the different sub-basins in terms of their overall $IC_{channel}$ (Fig. 6a) and IC_{outlet} (Fig. 6b) values excluding glaciers and lakes in the statistics. In conjucntion with the detailed statistical analysis (Tables 3 and 4) derived from the IC maps, the PD plots also help to understand the responses of the different sub basins in terms of sediment transfer. Both the plots show distinct patterns of PDs for all sub-basins based on IC range, but for some of the sub-basins, the plots overlap with each other. Both plots show positive skewness (i.e., high IC value distribution) for the entire upper Kosi basin (Fig. 7a, b, Tables 3 and 4). Therefore, the median of IC values is used to define the relative order of the sub-basins. Further, the quartiles, Q1 (0–25%), Q2 (25–50%), Q3 (50–75%) and Q4 (75–100%) define the area contribution of each sub-basin towards IC (Tables 3 and 4).

5. Discussion

5.1. Spatial distribution of connectivity

Mapping of $IC_{channel}$ (hillslope to channel) and IC_{outlet} (catchment connectivity) shows considerable spatial variation in the connectivity in the upper Kosi basin reflecting variable efficiency of sediment routing from different sub-basins. These differences can be linked to the various controlling factors that combine landscape properties (e.g. vegetation,

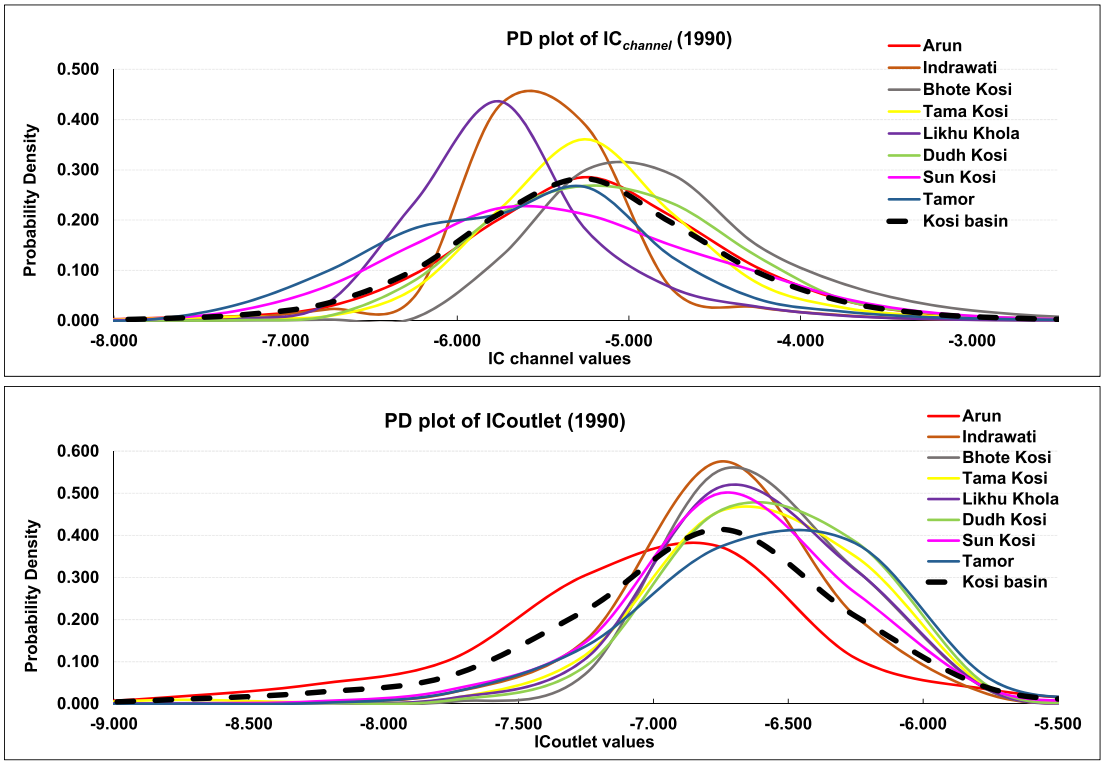

Fig. 7. Probability density (PD) plots of (a) $IC_{channel}$ (b) IC_{outlet} of upper Kosi basin.

morphology, slope, catchment area) with driving variables (e.g. rainfall intensity and its cumulative amount) and human activities (Fryirs et al., 2007a; Lexartza-Artza and Wainwright, 2011; Gumiere et al., 2011).

In general, the inhomogeneity across the different sub-basins is much more impressive in the $IC_{channel}$ compared with the IC_{outlet} map and this is also reflected from the statistics presented in Tables 3 and 4. The $IC_{channel}$ values for each sub-basin show a much higher standard deviation reflecting larger variability within each sub-basin and this also results in more significant contrast amongst them. Lower standard deviation in IC_{outlet} values and much lesser variability across the sub-basins result in a much more homogeneous map. Tables 3 and 4 also show a large variation in the median values of the $IC_{channel}$ compared to those of the IC_{outlet} across the sub-basins. The PD plots show a good separation of curves for the $IC_{channel}$. The Bhote Kosi and Dudh Kosi show peaks at higher $IC_{channel}$ values and the Indrawati and Likhu Khola show much lower values, and the values for the rest of the sub-basins fall in between. In contrast, the PD plots for the IC_{outlet} show a clustering for most sub-basins except for the Arun which shows a peak at much lower value.

Fig. 7 also shows the PD plot for the entire upper Kosi basin and Tables 3 and 4 show the percent contrubution of IC values for the four quartiles with respect to this curve for each sub-basin. For $IC_{channel}$, the Bhote Kosi and Dudh Kosi have higher contribution (~33–41%) from high IC values whereas the Likhu Khola and Indrawati have the lowest contribution (~7%). For IC_{outlet}, the Arun has the lowest percentage of contribution (~14%) from the high IC quartiles and Tamor (~45%) and Dudh Kosi (~43%) have the highest.

5.2. Controlling factors and field evidences

5.2.1. Controls on hillslope-channel connectivity ($IC_{channel}$)

The $IC_{channel}$ map (Fig. 6a) primarily reflects the connectivity between hillslope and channels, and thus, higher values adjacent to the main channels for most of the sub-basins reflect efficient sediment transfer from these slopes. In contrast, the hills and slopes far away from the channel show low $IC_{channel}$ values. In general, dense forest cover contributes to low sediment connectivity by stabilizing the steep slopes in a catchment (van Rompaey et al., 2002; Gomi et al., 2008; Schlunegger et al., 2009) which is the dominant factor that contributes to low $IC_{channel}$ in the sub-basins such as the Sun Kosi (~66%), Likhu Khola and Indrawati (~58%) and Tamor (48%) (Fig. 8a, b, c). It also reduces sediment transfer by decreasing erosion and increasing sedimentation (Sandercock and Hooke, 2011). The next dominant component of vegetation in the Kosi basin is grassland, which shows a bimodal behavior. The presence of grasslands in the high elevation areas with the steep slopes favors sediment connectivity as compared to grassland on the gentle slopes (Gomi et al., 2008; Kamarinas et al., 2016). In contrast, grassland reduces the runoff (up to 84%) in flat and poorly defined valleys (Schmidt and Morche, 2006; Le Bissonnais et al., 2004; Puigdefábregas, 2005). Experimental studies by Abujamin et al. (1984) have also demonstrated the runoff reduction up to 50–60% due to grasslands. The Arun has ~69% of the total basin area under grassland combining both the high upland areas of the central Himalaya and far north of the Tibetan plateau. As a result, the Tibetan part shows low $IC_{channel}$ values but the narrow and steep valleys of the Arun in the middle part have very high potential of transferring sediments into the channel (Fig. 9a), and this results in high $IC_{channel}$ values along the main channel (Fig. 6a).

The Bhote Kosi has a moderate (~44%) grassland cover but has the highest barren land (~13%). Studies have shown that agriculture (arable lands), shrubland and barren areas or badlands (semi-arid conditions) are amongst the highest contributor to sediment connectivity (up to 40%; Brosinsky et al., 2014) in high slope areas that intensify the hydrologic response on the hillslope due to the increasing elevational gradients with increasing slope angle (Hopp and McDonnell, 2009). A major landslide in the upslope area of the Bhote Kosi in 2014 (Jure landslide) formed a large dam with water depth in excess of 15 m filling up the entire valley. While the dam failed eventually, large amount of slide material still lies on the barren slope (Fig. 9b). Further upstream, large debris flows feeding into the channel are observed along the steep and barren slope of the Bhote Kosi (Fig. 9c) manifesting high $IC_{channel}$ values at these sites. Such basins with bare and/or crust areas on stony steep slopes are considered as the hotspots, generating quick runoff that triggers erosion immediately downstream in the pathway link (Marchamalo et al., 2016).

Several authors (e.g. Otto et al., 2009; Hoffmann et al., 2013) have suggested that ~60% of the sediment are still stored within the hanging valleys in mountainous areas since the last deglaciation due to their characteristic shape, size (<10 km^2) and topographic position. It is argued therefore that only a fraction of the sediments currently stored in the catchment and hill slopes will contribute to the sediment flux from the basin (Messenzehl et al., 2014) The presence of snow/glaciers and glacal lakes plays an important role in temporary trapping of sediments and they can release significant amount of sediments during the retreat phases. The Tama Kosi, Bhote Kosi and Dudh Kosi sub basins have ~10% of the total area under permanent snow/glacier followed by Tamor (~8%) and Arun (~6%) with Likhu Khola (~3%) and Indrawati (~2%) which contribute only a fraction of the total sediment in the freezing season (Nov–Jan). Although the IC computation does not consider the glaciated surfaces in terms of sediment release, this may be an important factor to assess the temporal variability in connectivity in such large basins particularly in context of melting of glaciers due to climate change.

5.2.2. Controls on catchment connectivity (IC_{outlet})

Catchment connectivity of a basin (IC_{outlet}) is controlled by its shape, size and channel gradient (Cavalli et al., 2013; D'Haen et al., 2013) as well as the intensity of the rainfall (Puigdefábregas, 2005). Several sub-basins such as the Sun Kosi, Likhu Khola, Indrawati, and Bhote Kosi have an elongate shape that leads to an increased sediment travel time from the hillslopes to the basin outlet once it reaches the channel, hampering the upstream-downstream linkage (Cavalli et al., 2013). As a

Fig. 8. Examples of low $IC_{channel}$: (a) vegetated slopes of the Indrawati river impeding sediment transfer from hill slopes, (b) vegetated, low slope regions along the Sun Kosi; (c) stable slope of Likhu Khola contributing little sediments to the channel.

Fig. 9. Examples of high $IC_{channel}$: (a) steep slope of Arun river with slopes covered with grassland; (b) barren/grassland covered slope along the Bhote Kosi allowing rapid sediment transfer; (c) completely barren slope along the Bhote Kosi that triggered Jure landslide in 2015; loose debris on the slopes are waiting to be mobilized into the channel.

consequence, they all show low IC_{outlet} values. In contrast, the circular shape of the Tama Kosi and the Dudh Kosi sub-basins allows a high and similar degree of connection between the steep hillslopes and the catchment outlet (Cavalli et al., 2013) and this is manifested in high IC_{outlet} values for these sub-basins (Fig. 10a, b). The Tamor and Arun show interesting situations. The Tamor is also an elongate sub-basin but the contributing area of well-connected parts of the basin is quite large, and hence, it shows the highest IC_{outlet} values in the uplands that serve as efficient sediment transfer systems (Fig. 10c). In contrast, the Arun is the largest sub-basin of all and this also has the lowest contribution from high IC quartiles (Table 4); this results in the lowest IC_{outlet} values for the Arun sub-basin.

Further, the channel slope gradually decreases with decrease in elevation and this impedes the sediment conveyance downstream to the outlet of the basin (Souza et al., 2016) as in the case of the Indrawati and the Likhu Khola (Fig. 11a). Very low values of slope in the midstream and downstream reaches of the Sun Kosi (Fig. 3a) are responsible for reduction in sediment conveyance to the outlet (Chatara). The Bhote Kosi, Tama Kosi, Dudh Kosi, and Arun show cascading longitudinal profiles in the upstream reaches (Fig. 4) typical of tectonically active regions where incision and dissection result in highly connected landscape with limited storage (Kuo and Brierley, 2013, 2014). The steeper river reaches such as those in the Dudh Kosi are generally associated with steep and narrow valleys (Fig. 10a) allowing a direct coupling between tributary valleys and the main river channel (Fryirs et al., 2007b; D'Haen et al., 2013). The Arun shows two contrasting morphologies i.e., U-shape valleys and low channel slope in the Tibetan part and V-shape valleys having high channel slope in the middle part (Fig. 9a) resulting into very low and moderate values of IC_{outlet} respectively. However, the total contributing area in terms of the moderate IC_{outlet} values (Q3 and Q4) in this largest sub-basin is very low (see Table 4) that reduces the sediment conveyance to the outlet and therefore a low IC_{outlet} value for the sub-basin. The slope profile of Tamor (Fig. 4e) shows a typical concave up profile followed by a gradual downstream decrease in slope. This is characterized by wider valleys in the midstream region of the Tamor, which hampers the connection with tributary and impedes the sediment transport.

5.3. Sediment connectivity and sediment dynamics

Table 5 summarises the overall response of the different sub basins to sediment connectivity based on the PD plot and also lists the major environmental controls in each case. In general, the dominant environmental factors that contribute to high sediment connectivity in the upper Kosi basin are land use and land cover change, steeply dissected terrain, the circular shape of the catchment, steep channel slope, and structurally controlled geology with low opportunities to store the eroded sediment in a well connected system (Bruijnzeel, 1990). Our analysis suggests that the overall response of the Arun sub-basin, the largest of all, to sediment connectivity is moderate. The Dudh Kosi, Tama Kosi, and Bhote Kosi, are amongst the most dynamic sub-basins with overall high sediment connectivity. The Indrawati, Likhu Khola, and Sun Kosi have overall low sediment connectivity whereas the Tamor shows an overall moderate connectivity.

The IC values are the function of topographic and land use characteristics, which helped us to understand impact of connectivity indices on sediment dynamics. However, hydrological forcing is also important in sediment mobilization. High-intensity rainfall triggers sediment erosion and produces events of peak discharge, which have important implications for sediment connectivity processes (Baartman et al., 2013). In terms of rainfall variability, the western part of the upper Kosi basin such as the Indrawati (1692 mm), Bhote Kosi (1065 mm), Tama Kosi (1028 mm), Likhu Khola (1295 mm) and Dudh Kosi (1175 mm) receive high annual rainfall which favors sediment mobilization in the mountainous area along with steep slopes (Michaelides and Wainwright, 2002). Further, the Arun is characterized by a major rainfall peak in its midstream area (Fig. 2).

Spatial rainfall variability within the upper Kosi basin was incorporated through stream power distribution pattern, which was derived through a hydrological model (SWAT) (Kaushal et al., in prep). The Arun River is chareacterised by high $IC_{channel}$ values. It has low longitudial connectivity for the basin area, however, the longitudinal connectivity in the midstream region is higher (Fig. 6a). The Dudh Kosi is also a highly connected system (Table 5). Both the river systems are also characterized by high to moderate stream power. A combination of good connectivity

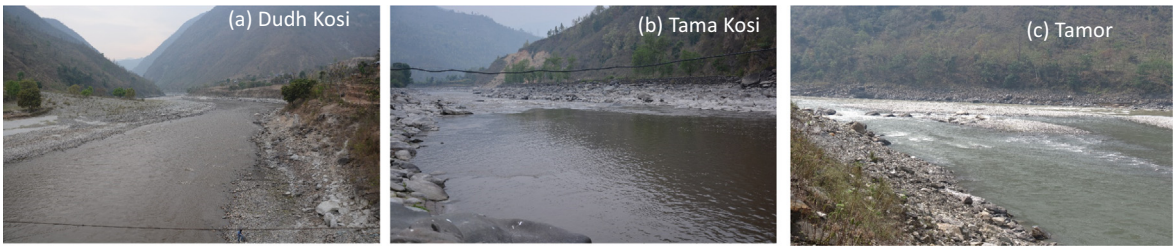

Fig. 10. Examples of high IC_{outlet}: (a) Dudh Kosi channel with abundant gravel and sand in the channel; highly turbid water reflecting high suspended load. (b) Tama Kosi channel with steep slopes and large boulder reflecting high longitudinal connectivity; (c) steep channels of Tamor as efficient sediment transfer system in the uplands.

Fig. 11. Examples of low IC_{outlet}: (a) complete choking of the Likhu Khola in the lower reaches due to moderate slope and low stream power; (b) large aggradational reaches in the Sun Kosi river reflecting poor longitudinal connectivity and low sediment conveyance capacity; (c) large wide valleys of Tamor with IC values showing sediment aggradation.

and higher stream power will be responsible for higher sediment supply from these river basins. Low connectivity and low stream power values of upstream area of the Arun River further suggest that sediment contribution from this area will be neglegible.

To understand the relationship between overall connectivity and sediment dynamics, we compare the sediment connectivity response with the limited sediment load estimates available for different sub basins (Table 1). The estimated sediment flux at the outlet of the upper Kosi basin measured at Chatara (immediately downstream of the cofluence of all tributaries, see Fig. 1) is ~101 million tonnes/year. The limited sediment load data (Table 1) suggests that the western tributaries (Bhote, Indrawati and Tama Kosi) contribute ~40 million tonnes annually (Sinha et al., 2019, in press). There are no independent estimates available for the Dudh Kosi but this suggests that atleast ~40% of the total sediment load at Chatara is being contributed by the western tributaries and this confirms our results that Bhote and Tama Kosi are amongst the most dynamic and well-connected system (Table 5). In contrast, the Tamor, the eastern tributary of the upper Kosi river basin, contributes only ~16% of the total sediment load at Chatara (Sinha et al., in press) (Table 1) and this is attributed to the presence of glaciers and high forest cover and low stream power values in midstream region that impede sediment transport from the upstream and midstream regions. This also provides some important insights in terms of future scenario of potential sediment dynamics. In particular, since glaciers are retreating, more sediment will be available for transfer processes, and sediments dynamics of these catchments may experience significant variations in the near future (with increased contributions to the main outlet).

The remaining ~44% of the total sediment load at Chatara is contributed from the Arun (largest basin with rainall peak and moderately connected, Table 5) and Dudh Kosi (highly connected system) for which no independent estimates of sediment load are available. In summary, the tributaries draining the middle part of the upper Kosi River basin not only produce large amounts of sediment but also have the ability to mobilized downstream because of high rainfall and high stream power compared to the northern part of the basin (Tibetan region).

6. Conclusions

In this study, a distributed index of sediment connectivity has been used in a large basin namely, the upper Kosi basin covering parts of Tibet and Nepal. This basin is characterized by contrasting LULC, and steep and dissected morphology that affect sediment remobilization from hillslopes to channel as well as along the channel to the basin outlet. The overall response of the Kosi basin towards sediment connectivity tends to be different in each of the sub-basins which is governed by the dominance of one controlling factor over the other. The sub-basins such as Dudh Kosi, Bhote Kosi, and Tama Kosi, are considered to be well connected as land use and land cover play an important role in mobilizing the sediments from source to the main channel along with longitudinal slope and morphology. In case of the Arun, the land-use along the steep and dissected terrain favors sediment movement, but the large size of the basin and variable slope reduces the contribution from far away areas. It also increases the travel time causing an overall moderate sediment connectivity. Although the Tamor shows high catchment connectivity, high forest cover percentage in the basin reduces the efficiency of sediment remobilization from hillslopes to channel, and therefore, this is categorised as an overall moderately connected system. The Indrawati, Sun Kosi, and Likhu Khola are elongate sub-basins, mostly dominated by forest cover that stabilizes the hillslopes and minimal channel gradient impedes sediment connectivity. We have also demonstrated that slope is not always the governing factor, but the LULC also influences the IC values significantly in the upper Kosi basin. However, within an individual LULC class, the IC values do not show a definite trend with increasing slope values.

Our connectivity analysis is well supported by limited sediment load data for some of the sub-basins. It is important however to note that the upper Kosi is a highly dynamic basin from the point of view of sediment production and transfer. Although this study has provided a first order assessment of structural sediment dynamics in the basin, it would be useful to analyse temporal variability in sediment connectivity of the basin in view of changing land use and land cover conditions as well

Table 5
Comparison table of the overall response to sediment connectivity of the upper Kosi basin.

Name of the basin	Hillslope to channel ($IC_{channel}$)	Catchment connectivity (IC_{outlet})	Inference (Overall response to connectivity)	Dominant environmental controls
Dudh Kosi	High	High	Highly connected system	Impact of land cover practices, steeply dissected terrains
Tama Kosi	High	Moderate	Highly connected system	Dissected terrains, steep slopes and high channel gradient
Bhote Kosi	High	Moderate	Highly connected system	Impact of land cover practices, steep and dissected terrains
Arun	High	Low	Moderately connected system	Large basin area, variable morphology from steep and dissected terrains to broad and U-shape valleys with poor and flat channel bed; grassland dominates in the upper part.
Tamor	Low	High	Moderately connected system	Dense forest cover, and impact of snow/glaciers
Indrawati	Low	Low	Poorly connected system	Small basin area next to Likhu Khola, gradual slope and impact of forest cover over other practices.
Sun Kosi	Moderate	Low	Poorly connected system	West to east alignment of the basin and elongate shape, riffle-pool sequences, dense forest cover
Likhu Khola	Low	Moderate	Poorly connected system	Smallest basin, elongate shape, dense vegetation cover.

as the periglacial dynamics due to increasing anthropogenic impacts in this region. This might lead to identification of new source areas of sediment production as well as mobilization pathways for designing sustainable sediment management strategies. The spatial variability in rainfall across the basin seems to exert significant influence on sediment mobilization and transport and this factor may be incorporated to assess the functional sediment connectivity in large basins. Another important area of further investigation is to understand the downstream impact of sediment connectivity in the alluvial plains including the influence of Kosi barrage and embankments on sediment aggradation and associated hazards such as avulsions and flooding.

Acknowledgments

This research, designed and implemented by ICIMOD's Koshi Basin Programme and its partner Indian Institute of Technology Kanpur contributes to the Sustainable Development Investment Portfolio and is supported by the Australia aid program. The ICIMOD gratefully acknowledges the support of its core donors: the governments of Afghanistan, Australia, Austria, Bangladesh, Bhutan, China, India, Myanmar, Nepal, Norway, Pakistan, Sweden, and Switzerland. A major part of this manuscript was prepared while one of the authors (RS) was supported by Alexander von Humboldt fellowship at University of Potsdam, Germany and this support is thankfully acknowledged. The views and interpretations in this publication are those of the authors and are not necessarily attributable to their organizations. The authors also thank the Indian Institute of Technology Kanpur for providing all necessary facilities for this work. This paper benefitted immensely from the critical comments of several annonymous reviewers and we thank them for their time and insights.

Appendix A. Supplementary data

Supplementary data to this article can be found online at https://doi.org/10.1016/j.scitotenv.2019.01.118.

References

Abujamin, S., Abdurachman, A., Suwardjo, M., 1984. Contour grass strips as a low-cost conservation practice. Proceedings of Conference on Soil Erosion and Its Countermeasures. 11–19 November 1984, Chiang Mai, Thailand.

Ali, G., Birkel, C., Tetzlaff, D., Soulsby, C., Mcdonnell, J.J., Tarolli, P., 2014. A comparison of wetness indices for the prediction of observed connected saturated areas under contrasting conditions. Earth Surf. Process. Landf. 39, 399–413. https://doi.org/10.1002/esp.3506.

Antoine, M., Javaux, M., Bielders, C., 2009. What indicators can capture runoff-relevant connectivity properties of the micro-topography at the plot scale? Adv. Water Resour. 32, 1297–1310. https://doi.org/10.1016/j.advwatres.2009.05.006.

Baartman, J.E.M., Masselink, R., Keesstra, S.D., Temme, A.J.A.M., 2013. Linking landscape morphological complexity and sediment connectivity. Earth Surf. Process. Landf. 38, 1457–1471. https://doi.org/10.1002/esp.3434.

Bajracharya, S.R., Mool, P.K., Shrestha, B.R., 2007. Impact of Climate Change on Himalayan Glaciers and Glacial Lakes: Case Studies on GLOF and Associated Hazards in Nepal and Bhutan. 169. ICIMOD Publ., p. 127.

Bookhagen, B., Strecker, M.R., 2012. Spatiotemporal trends in erosion rates across a pronounced rainfall gradient: examples from the southern Central Andes. Earth Planet. Sci. Lett. 327–328, 97–110. https://doi.org/10.1016/j.epsl.2012.02.005.

Borselli, L., Cassi, P., Torri, D., 2008. Prolegomena to sediment and flow connectivity in the landscape: a GIS and field numerical assessment. Catena 75, 268–277. https://doi.org/10.1016/j.catena.2008.07.006.

Bracken, L.J., Croke, J., 2007. The concept of hydrological connectivity and its contribution to understanding runoff-dominated geomorphic systems. Hydrol. Process. 21, 1749–1763. https://doi.org/10.1002/hyp.6313.

Bracken, L.J., Wainwright, J., Ali, G.A., Tetzlaff, D., Smith, M.W., Reaney, S.M., Roy, A.G., 2013. Concepts of hydrological connectivity: research approaches, pathways and future agendas. Earth Sci. Rev. 119, 17–34. https://doi.org/10.1016/j.earscirev.2013.02.001.

Bracken, L.J., Turnbull, L., Wainwright, J., Bogaart, P., 2015. Sediment connectivity: a framework for understanding sediment transfer at multiple scales. Earth Surf. Process. Landf. 40, 177–188. https://doi.org/10.1002/esp.3635.

Brierley, G., Fryirs, K., Jain, V., 2006. Landscape connectivity: the geographic basis of geomorphic applications. Area 38, 165–174. https://doi.org/10.1111/j.1475-4762.2006.00671.x.

Brosinsky, A., Foerster, S., Segl, K., Bronstert, A., 2014. Spectral Fingerprinting: characterizing suspended sediment sources by the use of VNIR-SWIR spectral information. , pp. 1965–1981 https://doi.org/10.1007/s11368-014-0927-z.

Bruijnzeel, L.A., 1990. Hydrology of moist tropical forests and effects of conversion: a state of knowledge review. Humid Tropics Programme of the International Hydrological Programme of UNESCO, Paris, and Vrije Universiteit, Amsterdam (224 pp.).

Brunsden, D., Thornes, J.B., 1979. Landscape sensitivity and change. Trans. Inst. Br. Geogr. 4, 463. https://doi.org/10.2307/622210.

Caine, N., Swanson, F.J., 1989. Geomorphic coupling of hillslope and channel systems in two small mountain basin. Z. Geomorphol. 33, 189–203.

Calsamiglia, A., García-Comendador, J., Fortesa, J., López-Tarazón, J.A., Crema, S., Cavalli, M., Calvo-Cases, A., Estrany, J., 2018. Effects of agricultural drainage systems on sediment connectivity in a small Mediterranean lowland catchment. Geomorphology 318, 162–171. https://doi.org/10.1016/j.geomorph.2018.06.011.

Casalí, J., Giménez, R., Díez, J., Álvarez-Mozos, J., Del Valle de Lersundi, J., Goñi, M., Campo, M.A., Chahor, Y., Gastesi, R., López, J., 2010. Sediment production and water quality of watersheds with contrasting land use in Navarre (Spain). Agric. Water Manag. 97, 1683–1694. https://doi.org/10.1016/j.agwat.2010.05.024.

Cavalli, M., Marchi, L., 2008. Characterisation of the surface morphology of an alpine alluvial fan using airborne LiDAR. Nat. Hazards Earth Syst. Sci. 8, 323–333. https://doi.org/10.5194/nhess-8-323-2008.

Cavalli, M., Trevisani, S., Comiti, F., Marchi, L., 2013. Geomorphometric assessment of spatial sediment connectivity in small Alpine catchments. Geomorphology 188, 31–41. https://doi.org/10.1016/j.geomorph.2012.05.007.

Cavalli, M., Crema, S., Blok, M., Lucía, A., Comiti, F., Marchi, L., 2016. Integrating structural and functional connectivity to characterize sediment dynamics in a small Alpine catchment. 18 p. 15034.

Chartin, C., Evrard, O., Onda, Y., Patin, J., Lefèvre, I., Ottlé, C., Ayrault, S., Lepage, H., Bonté, P., 2013. Tracking the early dispersion of contaminated sediment along rivers draining the Fukushima radioactive pollution plume. Anthropocene 1, 23–34. https://doi.org/10.1016/j.ancene.2013.07.001.

Cossart, É., Fressard, M., 2017. Assessment of structural sediment connectivity within catchments: insights from graph theory. Earth Surf. Dyn. 5, 253–268. https://doi.org/10.5194/esurf-5-253-2017.

Crema, S., Cavalli, M., 2018. SedInConnect: a stand-alone, free and open source tool for the assessment of sediment connectivity. Comput. Geosci. 111, 39–45. https://doi.org/10.1016/j.cageo.2017.10.009.

Dalla Fontana, G., Marchi, L., 2003. Slope-area relationships and sediment dynamics in two alpine streams. Hydrol. Process. 17, 73–87. https://doi.org/10.1002/hyp.1115.

Darboux, F., Davy, P., Gascuel-Odoux, C., Huang, C., 2001. Evolution of soil surface roughness and flowpath\connectivity in overland flow experiments. Catena 46, 125–139. https://doi.org/10.1016/S0341-8162(01)00162-X.

De Jong, S.M., 1994. Derivation of vegetative variables from a landsat tm image for modelling soil erosion. Earth Surf. Process. Landf. 19, 165–178. https://doi.org/10.1002/esp.3290190207.

Delmas, M., Cerdan, O., Mouchel, J.M., Garcin, M., 2009. A method for developing a large-scale sediment yield index for European river basins. J. Soils Sediments 9, 613–626. https://doi.org/10.1007/s11368-009-0126-5.

D'Haen, K., Dusar, B., Verstraeten, G., Degryse, P., De Brue, H., 2013. A sediment fingerprinting approach to understand the geomorphic coupling in an eastern Mediterranean mountainous river catchment. Geomorphology 197, 64–75. https://doi.org/10.1016/j.geomorph.2013.04.038.

Farraj, A.A.L., Harvey, A., 2010. Influence of hillslope-to-channel and tributary-junction coupling on channel morphology and sediments: Bowderdale Beck, Howgill Fells, NW England. Z. Geomorphol. 54, 203–224. https://doi.org/10.1127/0372-8854/2010/0054-0018.

Foerster, S., Wilczok, C., Brosinsky, A., Segl, K., 2014. Assessment of sediment connectivity from vegetation cover and topography using remotely sensed data in a dryland catchment in the Spanish Pyrenees. J. Soils Sediments 14, 1982–2000. https://doi.org/10.1007/s11368-014-0992-3.

Fryirs, K., 2013. (Dis)connectivity in catchment sediment cascades: a fresh look at the sediment delivery problem. Earth Surf. Process. Landf. 38, 30–46. https://doi.org/10.1002/esp.3242.

Fryirs, K.A., Brierley, G.J., Preston, N.J., Kasai, M., 2007a. Buffers, barriers and blankets: the (dis)connectivity of catchment-scale sediment cascades. Catena 70, 49–67. https://doi.org/10.1016/j.catena.2006.07.007.

Fryirs, K.A., Brierley, G.J., Preston, N.J., Spencer, J., 2007b. Catchment-scale (dis)connectivity in sediment flux in the upper Hunter catchment, New South Wales, Australia. Geomorphology 84, 297–316. https://doi.org/10.1016/j.geomorph.2006.01.044.

Gomi, T., Sidle, R.C., Miyata, S., Kosugi, K., Onda, Y., 2008. Dynamic runoff connectivity of overland flow on steep forested hillslopes: scale effects and runoff transfer. Water Resour. Res. 44, 1–16. https://doi.org/10.1029/2007WR005894.

Gumiere, S.J., Le Bissonnais, Y., Raclot, D., Cheviron, B., 2011. Vegetated filter effects on sedimentological connectivity of agricultural catchments in erosion modelling: a review. Earth Surf. Process. Landf. 36, 3–19. https://doi.org/10.1002/esp.2042.

Harvey, A.M., 2001. Coupling between hillslopes and channels in upland fluvial systems: implications for landscape sensitivity, illustrated from the Howgill Fells, northwest England. Catena 42, 225–250. https://doi.org/10.1016/S0341-8162(00)00139-9.

Hassan, M.A., Church, M., Schick, A.P.S., 1991. Distance of movement of coarse particles in gravel bed streams. Water Resour. Res. 27, 503–551. https://doi.org/10.1029/90WR02762.

Heckmann, T., Schwanghart, W., 2013. Geomorphic coupling and sediment connectivity in an alpine catchment - Exploring sediment cascades using graph theory. Geomorphology 182, 89–103. https://doi.org/10.1016/j.geomorph.2012.10.033.

Heckmann, T., Schwanghart, W., Phillips, J.D., 2014. Graph theory-recent developments of its application in geomorphology. Geomorphology 243, 130–146. https://doi.org/10.1016/j.geomorph.2014.12.024.

Hoffmann, T., Müller, T., Johnson, E.A., Martin, Y.E., 2013. Postglacial adjustment of steep, low-order drainage basins, Canadian Rocky Mountains. J. Geophys. Res. Earth Surf. 118, 2568–2584. https://doi.org/10.1002/2013JF002846.
Hooke, J.M., 2006. Human impacts on fluvial systems in the Mediterranean region. Geomorphology 79, 311–335. https://doi.org/10.1016/j.geomorph.2006.06.036.
Hopp, L., McDonnell, J.J., 2009. Connectivity at the hillslope scale: identifying interactions between storm size, bedrock permeability, slope angle and soil depth. J. Hydrol. 376, 378–391. https://doi.org/10.1016/j.jhydrol.2009.07.047.
Immerzeel, W.W., Van Beek, L.P.H., Bierkens, M.F.P., 2010. Climate change will affect the asian water towers. Science 328 (80), 1382–1385. https://doi.org/10.1126/science.1183188.
Kamarinas, I., Julian, J.P., Hughes, A.O., Owsley, B.C., de Beurs, K.M., 2016. Nonlinear changes in land cover and sediment runoff in a New Zealand catchment dominated by plantation forestry and livestock grazing. Water 8. https://doi.org/10.3390/w8100436.
Kaushal R.K., Sarkar A., Mishra K., Sinha R., Nepal S. and Jain V., SWAT Based Analysis of Spatio-temporal Variability in Stream Power Distribution, Upper Kosi River Basin, Central Himalaya, (in prep).
Keesstra, S.D., van Dam, O., Verstraeten, G., van Huissteden, J., 2009. Changing sediment dynamics due to natural reforestation in the Dragonja catchment, SW Slovenia. Catena 78, 60–71. https://doi.org/10.1016/j.catena.2009.02.021.
Keesstra, S., Kondrlova, E., Czajka, A., Seeger, M., Maroulis, J., 2012. Assessing riparian zone impacts on water and sediment movement: a new approach. Neth. J. Geosci. 91 (1–2), 245–255. https://doi.org/10.1017/S0016774600001633.
Korup, O., 2005. Geomorphic imprint of landslides on alpine river systems, southwest New Zealand. Earth Surf. Process. Landf. 30, 783–800. https://doi.org/10.1002/esp.1171.
Kumar, R., Jain, V., Prasad Babu, G., Sinha, R., Babu, G.P., Sinha, R., Prasad Babu, G., Sinha, R., 2014. Connectivity structure of the Kosi megafan and role of rail-road transport network. Geomorphology 227, 73–86. https://doi.org/10.1016/j.geomorph.2014.04.031.
Kuo, C.W., Brierley, G.J., 2013. The influence of landscape configuration upon patterns of sediment storage in a highly connected river system. Geomorphology 180–181, 255–266. https://doi.org/10.1016/j.geomorph.2012.10.015.
Kuo, C.W., Brierley, G., 2014. The influence of landscape connectivity and landslide dynamics upon channel adjustments and sediment flux in the Liwu Basin, Taiwan. Earth Surf. Process. Landf. 39, 2038–2055. https://doi.org/10.1002/esp.3598.
Lane, S.N., Reaney, S.M., Heathwaite, A.L., 2009. Representation of landscape hydrological connectivity using a topographically driven surface flow index. Water Resour. Res. 45. https://doi.org/10.1029/2008WR007336 (n/a-n/a).
Le Bissonnais, Y., Lecomte, V., Cerdan, O., 2004. Grass strip effects on runoff and soil loss. Agronomie 24, 129–136. https://doi.org/10.1051/agro:2004010.
Lexartza-Artza, I., Wainwright, J., 2011. Making connections: changing sediment sources and sinks in an upland catchment. Earth Surf. Process. Landf. 36, 1090–1104. https://doi.org/10.1002/esp.2134.
Liébault, F., Gomez, B., Page, M., Marden, M., Peacock, D., Richard, D., Trotter, C.M., 2005. Land-use change, sediment production and channel response in upland regions. River Res. Appl. 21, 739–756. https://doi.org/10.1002/rra.880.
López-Vicente, M., Poesen, J., Navas, A., Gaspar, L., 2013. Predicting runoff and sediment connectivity and soil erosion by water for different land use scenarios in the Spanish Pre-Pyrenees. Catena 102, 62–73. https://doi.org/10.1016/j.catena.2011.01.001.
Macklin, M.G., Lewin, J., 2009. Alluvial responses to the changing Earth system. Earth Surf. Process. Landf. 34, 155–161. https://doi.org/10.1002/esp.
Mao, L., Cavalli, M., Comiti, F., Marchi, L., Lenzi, M.A., Arattano, M., 2009. Sediment transfer processes in two Alpine catchments of contrasting morphological settings. J. Hydrol. 364, 88–98. https://doi.org/10.1016/j.jhydrol.2008.10.021.
Marchamalo, M., Hooke, J.M., Sandercock, P.J., 2016. Flow and sediment connectivity in semi-arid landscapes in SE Spain: patterns and controls. Land Degrad. Dev. 27, 1032–1044. https://doi.org/10.1002/ldr.2352.
Marchi, L., Dalla Fontana, G., 2005. GIS morphometric indicators for the analysis of sediment dynamics in mountain basins. Environ. Geol. 48, 218–228. https://doi.org/10.1007/s00254-005-1292-4.
Marden, M., Arnold, G., Gomez, B., Rowan, D., 2005. Pre- and post-reforestation gully development in Mangatu Forest, East Coast, North Island, New Zealand. River Res. Appl. 21, 757–771. https://doi.org/10.1002/rra.882.
Mekonnen, M., Keesstra, S.D., Baartman, J.E.M., Stroosnijder, L., Maroulis, J., 2014. Soil conservation through sediment trapping: a review. Land Degrad. Dev. 26, 544–556. https://doi.org/10.1002/ldr.2308.
Messenzehl, K., Hoffmann, T., Dikau, R., 2014. Sediment connectivity in the high-alpine valley of Val Müschauns, Swiss National Park - linking geomorphic field mapping with geomorphometric modelling. Geomorphology 221, 215–229. https://doi.org/10.1016/j.geomorph.2014.05.033.
Michaelides, K., Wainwright, J., 2002. Modelling the effects of hillslope-channel coupling on catchment hydrological response. Earth Surf. Process. Landf. 27, 1441–1457. https://doi.org/10.1002/esp.440.
Montgomery, D.R., Dietrich, W.E., 1989. Source areas, drainage density, and channel initiation. Water Resour. Res. 25 (8), 1907–1918. https://doi.org/10.1029/WR025i008p01907.
Nicholas, A.P., Ashworth, P.J., Kirkby, M.J., Macklin, M.G., Murray, T., 1995. Sediment slugs: large-scale fluctuations in fluvial sediment transport rates and storage volumes. Prog. Phys. Geogr. 19, 500–519. https://doi.org/10.1177/030913339501900404.
Otto, J.C., Schrott, L., Jaboyedoff, M., Dikau, R., 2009. Quantifying sediment storage in a high alpine valley (Turtmanntal, Switzerland). Earth Surf. Process. Landf. 34, 1726–1742. https://doi.org/10.1002/esp.1856.
Pan, C., Ma, L., Shangguan, Z., Ding, A., 2011. Determining the sediment trapping capacity of grass filter strips. J. Hydrol. 405, 209–216. https://doi.org/10.1016/j.jhydrol.2011.05.027.
Pavanelli, D., Cavazza, C., 2010. River suspended sediment control through riparian vegetation: a method to detect the functionality of riparian vegetation. Clean: Soil, Air, Water 38, 1039–1046. https://doi.org/10.1002/clen.201000016.
Persichillo, M.G., Bordoni, M., Meisina, C., Bartelletti, C., Barsanti, M., Giannecchini, R., D'Amato Avanzi, G., Galanti, Y., Cevasco, A., Brandolini, P., Galve, J.P., 2017. Shallow landslides susceptibility assessment in different environments. Geomat. Nat. Haz. Risk 8, 748–771. https://doi.org/10.1080/19475705.2016.1265011.
Poeppl, R.E., Keiler, M., Von Elverfeldt, K., Zweimueller, I., Glade, T., 2012. The influence of riparian vegetation cover on diffuse lateral sediment connectivity and biogeomorphic processes in a medium-sized agricultural catchment, Austria. Geogr. Ann. A 94, 511–529. https://doi.org/10.1111/j.1468-0459.2012.00476.x.
Puigdefábregas, J., 2005. The role of vegetation patterns in structuring runoff and sediment fluxes in drylands. Earth Surf. Process. Landf. 30, 133–147. https://doi.org/10.1002/esp.1181.
Reid, S.C., Lane, S.N., Montgomery, D.R., Brookes, C.J., 2007. Does hydrological connectivity improve modelling of coarse sediment delivery in upland environments? Geomorphology 90, 263–282. https://doi.org/10.1016/j.geomorph.2006.10.023.
Roth, G., La Barbera, P., Greco, M., 1996. On the description of the basin effective drainage structure. J. Hydrol. 187, 119–135. https://doi.org/10.1016/S0022-1694(96)03090-9.
Roy, A., Lamarre, H., 2011. Fluids, flows and fluxes in geomorphology. In: Gregory, K., Goudie, A. (Eds.), The SAGE Handbook of Geomorphology. SAGE Publications Ltd., London, pp. 310–325 https://doi.org/10.4135/9781446201053.n18.
Sandercock, P.J., Hooke, J.M., 2011. Vegetation effects on sediment connectivity and processes in an ephemeral channel in SE Spain. J. Arid Environ. 75 (3), 239–254. https://doi.org/10.1016/j.jaridenv.2010.10.005.
Schlunegger, F., Badoux, A., McArdell, B.W., Gwerder, C., Schnydrig, D., Rieke-Zapp, D., Molnar, P., 2009. Limits of sediment transfer in an alpine debris-flow catchment, Illgraben, Switzerland. Quat. Sci. Rev. 28, 1097–1105. https://doi.org/10.1016/j.quascirev.2008.10.025.
Schmidt, K.H., Morche, D., 2006. Sediment output and effective discharge in two small high mountain catchments in the Bavarian Alps, Germany. Geomorphology 80, 131–145. https://doi.org/10.1016/j.geomorph.2005.09.013.
Singh, M., Sinha, R., 2019. Evaluating dynamic hydrological connectivity of a floodplain wetland in North Bihar, India using geostatistical methods. Sci. Total Environ. 651, 2473–2488. https://doi.org/10.1016/j.scitotenv.2018.10.139.
Singh, M., Tandon, S.K., Sinha, R., 2017. Assessment of connectivity in a water-stressed wetland (Kaabar Tal) of Kosi-Gandak interfan, north Bihar Plains, India. Earth Surf. Process. Landf. 42, 1982–1996. https://doi.org/10.1002/esp.4156.
Sinha, R., Gaurav, K., Chandra, S., Tandon, S.K., 2013. Exploring the channel connectivity structure of the August 2008 avulsion belt of the Kosi River, India: application to flood risk assessment. Geology 41, 1099–1102. https://doi.org/10.1130/G34539.1.
Sinha, R., Priyanka, S., Jain, V., Mukul, Malay, 2014. Avulsion threshold and planform dynamics of the Kosi river in north Bihar (India) and Nepal: a GIS framework. Geomorphology 216, 157–170. https://doi.org/10.1016/j.geomorph.2014.03.035.
Sinha, R., Gupta, A., Mishra, K., Tripathi, S., Nepal, S., Wahid, S.M., Swarnkar, S., 2019. Basin scale hydrology and sediment dynamics of the Kosi River in the Himalayan foreland. J. Hydrol. https://doi.org/10.1016/j.jhydrol.2018.12.05 (in press).
Sougnez, N., van Wesemael, B., Vanacker, V., 2011. Low erosion rates measured for steep, sparsely vegetated catchments in southeast Spain. Catena 84, 1–11. https://doi.org/10.1016/j.catena.2010.08.010.
Souza, J.O.P., Correa, A.C.B., Brierley, G.J., 2016. An approach to assess the impact of landscape connectivity and effective catchment area upon bedload sediment flux in Saco Creek Watershed, Semiarid Brazil. Catena 138, 13–29. https://doi.org/10.1016/j.catena.2015.11.006.
Tarboton, D., 1997. A new method for the determination of flow directions and upslope areas in grid digital elevation models. Water Resour. Res. 33, 309–319.
Theler, D., Reynard, E., Lambiel, C., Bardou, E., 2010. The contribution of geomorphological mapping to sediment transfer evaluation in small alpine catchments. Geomorphology 124, 113–123. https://doi.org/10.1016/j.geomorph.2010.03.006.
Turnbull, L., Wainwright, J., Brazier, R.E., 2008. A conceptual framework for understanding semi- arid land degradation: ecohydrological interactions across multiple-space and time scales. Ecohydrology 1, 23–34. https://doi.org/10.1002/eco.4.
Uddin, K., Shrestha, H.L., Murthy, M.S.R., Bajracharya, B., Shrestha, B., Gilani, H., Pradhan, S., Dangol, B., 2015. Development of 2010 national land cover database for the Nepal. J. Environ. Manag. 148, 82–90. https://doi.org/10.1016/j.jenvman.2014.07.047.
Uddin, K., Murthy, M.S.R., Wahid, S.M., Matin, M.A., 2016. Estimation of soil erosion dynamics in the Koshi Basin using GIS and remote sensing to assess priority areas for conservation. PLoS One 11, e0150494. https://doi.org/10.1371/journal.pone.0150494.
Van Rompaey, A.J.J., Govers, G., Puttemans, C., 2002. Modelling land use changes and their impact on soil erosion and sediment supply to rivers. Earth Surf. Process. Landf. 27, 481–494. https://doi.org/10.1002/esp.335.
Vigiak, O., Borselli, L., Newham, L.T.H., McInnes, J., Roberts, A.M., 2012. Comparison of conceptual landscape metrics to define hillslope-scale sediment delivery ratio. Geomorphology 138, 74–88. https://doi.org/10.1016/j.geomorph.2011.08.026.
Walling, D.E., 1983. The sediment delivery problem. J. Hydrol. 65, 209–237. https://doi.org/10.1016/0022-1694(83)90217-2.
Walling, D.E., Collins, A.L., 2008. The catchment sediment budget as a management tool. Environ. Sci. Pol. 11, 136–143. https://doi.org/10.1016/j.envsci.2007.10.004.
Ward, P.J., van Balen, R.T., Verstraeten, G., Renssen, H., Vandenberghe, J., 2009. The impact of land use and climate change on late Holocene and future suspended sediment yield of the Meuse catchment. Geomorphology 103, 389–400. https://doi.org/10.1016/j.geomorph.2008.07.006.
Western, A.W., Blöschl, G., Grayson, R.B., 2001. Toward capturing hydrologically significant connectivity in spatial patterns. Water Resour. Res. 37, 83–97. https://doi.org/10.1029/2000WR900241.
Yatagai, A., Kamiguchi, K., Arakawa, O., Hamada, A., Yasutomi, N., Kitoh, A., 2012. Aphrodite constructing a long-term daily gridded precipitation dataset for Asia based on a dense network of rain gauges. Bull. Am. Meteorol. Soc. 93, 1401–1415. https://doi.org/10.1175/BAMS-D-11-00122.1.